

Liquid-liquid phase separation and viscosity within secondary organic aerosol generated from diesel fuel vapors

Mijung Song^{1,2}, Adrian M. Maclean², Yuanzhou Huang², Natalie R. Smith³, Sandra L. Blair³, Julia Laskin⁴, Alexander Laskin⁴, Wing-Sy Wong DeRieux³, Ying Li³, Manabu Shiraiwa³, Sergey A. Nizkorodov³, Allan K. Bertram^{2*}

[1] {Department of Earth and Environmental Sciences, Chonbuk National University, Jeollabuk-do, 54896, Republic of Korea}

[2] {Department of Chemistry, University of British Columbia, Vancouver, BC, V6T 1Z1, Canada}

[3] {Department of Chemistry, University of California Irvine, Irvine, CA 92697, USA}

[4] {Department of Chemistry, Purdue University, West Lafayette, IN 47907, USA}

Abstract

Information on liquid-liquid phase separation (LLPS) and viscosity (or diffusion) within secondary organic aerosol (SOA) is needed to improve predictions of particle size, mass, reactivity, and cloud nucleating properties in the atmosphere. Here we report on LLPS and viscosities within SOA generated by the photooxidation of diesel fuel vapors. Diesel fuel contains a wide range of volatile organic compounds, and SOA generated by the photooxidation of diesel fuel vapors may be a good proxy for SOA from anthropogenic emissions. In our experiments, LLPS occurred over the relative humidity (RH) range of ~70 % to ~100 %, resulting in an organic-rich outer phase and a water-rich inner phase. These results may have implications for predicting the cloud nucleating properties of anthropogenic SOA since the presence of an organic-rich outer phase at high RH values can lower the supersaturation with respect to water required for cloud droplet formation. At ≤ 10 % RH, the viscosity was $\geq 1 \times 10^8$ Pa s, which corresponds to roughly the viscosity of tar pitch. At 38 - 50 % RH the viscosity was in the range of 1×10^8 - 3×10^5 Pa s. These measured viscosities are consistent with predictions based on oxygen to carbon elemental ratio (O:C) and molar mass as well as predictions based on the number of carbon, hydrogen, and oxygen atoms. Based on the measured viscosities and the Stokes-Einstein relation, at ≤ 10 % RH diffusion coefficients of organics within diesel fuel SOA is $\leq 5.4 \times 10^{-17}$ cm² s⁻¹ and the mixing time of organics within

1 200 nm diesel fuel SOA particles (τ_{mixing}) is ≥ 50 h. These small diffusion coefficients and large
2 mixing times may be important in laboratory experiments, where SOA is often generated and
3 studied using low RH conditions and on time scales of minutes to hours. At 38 - 50 % RH, the
4 calculated organic diffusion coefficients are in the range of 5.4×10^{-17} to 1.8×10^{-13} cm² s⁻¹ and
5 calculated τ_{mixing} values are in the range of ~0.01 h to ~50 h. These values provide important
6 constraints for the physicochemical properties of anthropogenic SOA.

7 8 **1 Introduction**

9 Volatile organic compounds (VOCs) are emitted into the atmosphere from both biogenic and
10 anthropogenic sources (Kanakidou et al., 2005; Hallquist et al., 2009). These VOCs can be
11 oxidized in the atmosphere, and the oxidized products can form secondary organic aerosol
12 (SOA) (Hallquist et al., 2009; Ervens et al., 2011). SOA accounts for 20 – 80 % of the mass of
13 atmospheric aerosol particles (Zhang et al., 2007; Jimenez et al., 2009) and plays an important
14 role in climate, air quality, and public health (Kanakidou et al., 2005; Jang et al., 2006; Solomon,
15 2007; Baltensperger et al., 2008; Murray et al., 2010; Wang et al., 2012; Pöschl and Shiraiwa,
16 2015; Shiraiwa et al., 2017; Shrivastava et al., 2017). Despite the importance of SOA, many of
17 the physicochemical properties of SOA remain poorly understood.

18 One physicochemical property of SOA that remains insufficiently understood is liquid-liquid
19 phase separation (LLPS) (Pankow, 2003; Marcolli and Krieger, 2006; Ciobanu et al., 2009;
20 Bertram et al., 2011; Krieger et al., 2012; Song et al., 2012a; Zuend and Seinfeld, 2012; Veghte
21 et al., 2013; You et al., 2014; O'Brien et al., 2015; Freedman, 2017). Very recent work has
22 shown that SOA particles free of inorganic salts can undergo LLPS at a high relative humidity
23 (RH) with implications for predicting the cloud nucleating properties of SOA (Petters et al.,
24 2006; Hodas et al., 2016; Renbaum-Wolff et al., 2016; Ovadnevaite et al., 2017; Rastak et al.,
25 2017; Song et al., 2017; Altaft et al., 2018; Liu et al., 2018; Song et al., 2018; Davies et al.,
26 2019; Ham et al., 2019). Several of these recent studies investigated SOA generated from a
27 single VOC (e.g., α -pinene or isoprene). However, in the atmosphere, SOA is formed from a
28 complex mixture of VOCs (Odum et al., 1997; Schauer et al., 2002a; 2002b; Vutukuru et al.,
29 2006; Velasco et al., 2007; de Gouw et al., 2008; Velasco et al., 2009; Gentner et al., 2012; Liu
30 et al., 2012; Hayes et al., 2015). Additional studies are needed to determine if SOA generated
31 from a complex mixture of VOCs of atmospheric relevance can also undergo LLPS at high RH.

1 Another physicochemical property of SOA that remains poorly understood is viscosity.
2 Viscosity together with the Stokes-Einstein equation can be used to predict diffusion rates of
3 organics within SOA, which can critically impact a number of processes involving SOA. For
4 example, diffusion of organics within SOA can impact particle size distributions (Shiraiwa et
5 al., 2013a; Zaveri et al., 2014; Zaveri et al., 2018) and particle mass concentrations (Shiraiwa
6 and Seinfeld, 2012; Ye et al., 2016; Yli-Juuti et al., 2017; Kim et al., 2019) in the atmosphere.
7 Diffusion rates within SOA can also affect multi-phase reactions (Shiraiwa et al., 2011; Zhou
8 et al., 2013; Steimer et al., 2014; Houle et al., 2015; Li et al., 2018), the extent of long-range
9 transport of pollutants (Zelenyuk et al., 2012; Zhou et al., 2013; Shrivastava et al., 2017; Mu
10 et al., 2018), ice nucleation (Murray et al., 2010; Wang et al., 2012; Wilson et al., 2012; Ladino
11 et al., 2014; Schill et al., 2014; Knopf et al., 2018), and crystalline of salts (Murray, 2008;
12 Murray and Bertram, 2008; Bodsworth et al., 2010; Song et al., 2013; Ji et al., 2017; Wang et
13 al., 2017).

14 Recently, a number of studies have investigated viscosity or diffusion rates within SOA
15 particles generated in the laboratory (Virtanen et al., 2010; Cappa et al., 2011; Perraud et al.,
16 2012; Saukko et al., 2012; Abramson et al., 2013; Robinson et al., 2013; Renbaum-Wolff et al.,
17 2013; Loza et al., 2013; Kidd et al., 2014; Pajunoja et al., 2014; Bateman et al., 2015; Li et al.,
18 2015; Song et al., 2015; Wang et al., 2015; Zhang et al., 2015; Grayson et al., 2016; Liu et al.,
19 2016; Song et al., 2016a; Ye et al., 2018; Ullmann et al., 2019). Almost all of these studies
20 focused on SOA generated from a single VOC. Additional studies that quantify the viscosity
21 of SOA generated from a complex mixture of VOCs of atmospheric relevance are also needed.
22 Functional group contribution methods have recently been used to predict viscosities within
23 organic matrices of atmospheric relevance (Song et al., 2016a; Song et al., 2016b; Grayson et
24 al., 2017; Rothfuss and Petters, 2017). Methods have also been developed to predict the glass
25 transition temperature and viscosity within an organic matrix of atmospheric relevance using
26 molar mass and oxygen to carbon elemental ratio (O:C) (Shiraiwa et al., 2017) or the number
27 of carbon, hydrogen, and oxygen atoms of the organic compounds within the organic matrix
28 (DeRieux et al., 2018). These methods, if accurate, should be useful for predicting viscosity of
29 SOA particles in the atmosphere.

30 Diesel fuel contains a wide range of VOCs including aromatics and alkanes. Furthermore, SOA
31 generated from the photooxidation of diesel fuel vapors may be a good proxy for SOA from
32 anthropogenic emissions (Odum et al., 1997; Schauer et al., 2002a; 2002b; Vutukuru et al.,

1 2006; Velasco et al., 2007; Velasco et al., 2009; de Gouw et al., 2008; Gentner et al., 2012; Liu
2 et al., 2012; Jathar et al., 2013; Jathar et al., 2014; Hayes et al., 2015; Blair et al., 2017; Gentner
3 et al., 2017; Jathar et al., 2017). In this study, we investigate LLPS and viscosity within SOA
4 particles generated by photooxidation of diesel fuel vapors. Measured viscosities are also
5 compared with predicted viscosities based on the methods developed by Shiraiwa et al. (2017)
6 and DeRieux et al. (2018). Based on the measured viscosities and the Stokes-Einstein relation,
7 diffusion coefficients and mixing times of large organic molecules within diesel fuel SOA were
8 also estimated.

9 10 **2 Experimental**

11 **2.1 SOA generation**

12 SOA from the photooxidation of diesel fuel vapors was produced in an identical manner to that
13 described previously (DSL/NO_x in Table 1 of Blair et al. (2017)). 45 μL of H₂O₂ (30 wt %) was
14 evaporated in a 5.6 m³ inflatable Teflon chamber to achieve a mixing ratio of 2 parts per million
15 by volume (ppmv). A mixture of NO in N₂ was injected from a gas cylinder to achieve 0.26
16 ppmv of NO in the chamber. A volume of 200 μL of Fluka. No. 2 diesel (UST-148, 50 mg mL⁻¹
17 solution of diesel in dichloromethane) was evaporated in the chamber, resulting in a
18 concentration of 1.8 mg m⁻³ organic vapor from diesel and a mixing ratio of 0.22 ppmv (based
19 on an average molecular weight of 200 g mol⁻¹ (Blair et al., 2017) and assuming no wall loss).
20 No seed aerosol was used, and the chamber RH was below 2%. UV-B lamps (FS40T12/UVB,
21 Solarc Systems Inc.) were used to drive the photooxidation, which lasted for 3 h, followed by
22 particle collection. After 3 h of photooxidation, the particle mass loading in the chamber was
23 550 μg m⁻³ based on measurements with a scanning mobility particle sizer (SMPS; TSI 3080
24 Electrostatic Classifier and TSI 3775 Condensation Particle Counter). An Aerodyne time-of-
25 flight aerosol mass spectrometer (ToF-AMS) was used to measure the particle mass spectra in
26 V mode. ToF-AMS data was analyzed using Squirrel version 1.61. For elemental analysis we
27 relied on the improved-ambient method by Canagaratna et al. (2015). Figure S1 shows typical
28 particle number concentration, mass concentration, and average atomic ratios during the
29 photooxidation. The O:C values (0.4 to 0.5) were consistent with O:C values reported by Blair
30 et al. (2017) for identically prepared samples.

31 For the LLPS and viscosity measurements, the SOA from the chamber was collected on
32 hydrophobic glass slides (12 mm coverslips, Hampton Research, Canada) for 120 min using

1 an inertial impactor. To make the surface of the glass slides hydrophobic, they were coated with
2 trichloro(1*H*,1*H*,2*H*,2*H*-perfluorooctyl)silane (Sigma-Aldrich) following the procedure
3 reported in Knopf (2003). After collection, the sizes of the SOA particles on the hydrophobic
4 glass slides were > 10 μm. These large sizes were formed by impaction and coagulation of the
5 SOA during collection.

6 7 **2.2. Measurements of LLPS**

8 SOA was collected on hydrophobic glass slides by impaction, resulting in SOA particles on the
9 hydrophobic glass slides with diameters > 10 μm and a spherical cap geometry. LLPS was
10 detected using an optical microscope (Zeiss Epiplan 10X/0.20 HD) coupled to a flow-cell with
11 temperature and RH control (Parsons et al., 2004; Pant et al., 2006; Song et al., 2012b). During
12 the experiments, a constant flow (1.5 L min⁻¹) of humidified N₂ gas was maintained within the
13 flow-cell and measured with a dew point hygrometer (General Eastern M4/E4 Dew Point
14 Monitor, Canada). The temperature within the flow-cell was maintained at 290 ± 1 K and
15 measured with a thermocouple (OMEGA, Canada). At the beginning of the experiments, the
16 SOA particles were equilibrated at around 100 % RH for at least 15 min. At this point, the focus
17 of the microscope was adjusted so the focal plane of the microscope corresponded to the top
18 or interior of several SOA particles. Due to the different sizes of the SOA particles on the
19 hydrophobic glass slides, the focal plane of the microscope corresponded to the top of some
20 SOA particles and the middle of some SOA particles while some smaller particles were not in
21 the focal plane (leading to blurry images). Next, the RH was reduced at a rate of 0.5% RH min⁻¹
22 until a value close to 0% was reached. While the RH was decreased, images of the particles
23 were acquired every 10 sec with a CCD camera connected to the microscope. From the images,
24 the number of phases (e.g. one phase or two phases) present in the particles were determined.
25 Typically the focus of the microscope was not adjusted as the RH was reduced. As the RH was
26 reduced, the size of the SOA particles decreased due to the loss of water, and some SOA
27 particles that were in focus at high RH values became out of focus at low RH values.

28 29 **2.3 Measurements of particle viscosity**

30 The viscosity of the collected particles was determined using the poke-and-flow technique,
31 which has been described by Renbaum-Wolff et al. (2013) and Grayson et al. (2015), and based,
32 in part, on the earlier experiments by Murray et al. (2012). In short, the SOA particles collected

1 on hydrophobic glass slides were placed inside a flow-cell with RH and temperature control
2 (Pant et al., 2006; Bertram et al., 2011; Song et al., 2012a). After conditioning the particles to
3 a known RH at 294 ± 1 K, the particles were poked with a sharp needle (~ 10 μm for the tip of
4 the needle) (Becton-Dickson, USA). The movement of the needle was controlled with a
5 micromanipulator (Narishige, model MO-202U, Japan). The change in morphology as a
6 function of time after poking the particles with the needle was recorded with a camera attached
7 to the microscope. From the morphology changes and fluid dynamics simulations, upper and
8 lower limits to the SOA viscosity were determined. Fluid dynamics simulations were
9 performed using the finite-element analysis software package, *COMSOL Multiphysics*
10 (Renbaum-Wolff et al., 2013; Grayson et al., 2015). The geometry used in the simulations was
11 based on the geometry of the particles after poking them with a needle. Additional details of
12 the poke-and-flow experiments and the fluid dynamics simulations are discussed in Sect. 3.2
13 and Sect. S1-S3 of the Supplement.

14 We acknowledge that viscosity of the SOA could change between the time of its initial
15 formation in the chamber and the time of the off-line viscosity and LLPS measurements. Such
16 changes can be driven by both evaporative losses and slow chemical aging processes. During
17 the MOUDI sampling, impacted particles are surrounded by the same gaseous products as in
18 the chamber and should not evaporate. We expect the evaporation to be minimal when the
19 collected particles are briefly exposed to ambient air, sealed in a storage container with a small
20 head space volume (~ 2 cm^3), and frozen for storage and shipment. However, in the poke-and-
21 flow experiments (as well as the LLPS experiments), the particles are exposed to a constant
22 flow of purified air at room temperature for an extended period of time which can lead to a
23 change in the composition of the particles by partitioning of semi-volatiles to the gas phase.
24 For a 1 hr poke-and-flow experiment, the amount of gas exposed to the SOA is 30 L compared
25 to 380 L collected from the environmental chamber. For a 27 hr poke-and-flow experiment
26 (maximum amount of time a sample was exposed to a constant gas flow), the amount of gas
27 exposed to the SOA was 810 L compared to 380 L collected from the environmental chamber.
28 We did not observe a relationship between particle viscosity and time the SOA was exposed to
29 a constant flow of gas in our experiments; however, semi-volatiles may still have evaporated
30 in the experiments when the particles were conditioned to a known RH and during the poke-
31 and-flow measurements. The loss of semi-volatiles would lead to an increase in viscosity of
32 the SOA (Wilson et al., 2015; Yli-Juuti et al., 2017; Buchholz et al., 2019). Consequently, our

1 results should be considered as upper limits to the viscosity of the SOA generated with a particle
2 mass loading of $550 \mu\text{g m}^{-3}$. The evaporation of semi-volatiles in the experiments as well as
3 possible slow chemical aging reactions occurring during shipment and storage may in fact have
4 resulted in the SOA being more similar to the chemical composition of SOA in the atmosphere,
5 which are formed at particle mass loadings $< 550 \mu\text{g m}^{-3}$ and then chemically aged.

6 7 **2.4 Predictions of viscosity based on high-resolution mass spectrometry**

8 Viscosities of the diesel fuel SOA was predicted using the elemental composition of the SOA
9 and the methods developed by Shiraiwa et al. (2017) and DeRieux et al. (2018). The elemental
10 compositions of the diesel fuel SOA were taken from a previous study (Blair et al., 2017) using
11 of SOA generated with identical conditions (DSL/NO_x Table 1 of Blair et al. (2017)). In the
12 previous study by Blair et al. (2017) high-resolution nanospray desorption electrospray
13 ionization mass spectrometry (Roach et al., 2010) was used to determine the elemental
14 composition.

15 Shiraiwa et al. (2017) reported a parameterization (Eq. 1) to estimate the glass transition
16 temperature (T_g) of individual CH or CHO compounds with molar mass $< \sim 450 \text{ g mol}^{-1}$.

$$17$$
$$18 T_g = A + BM + CM^2 + D (\text{O:C}) + E M (\text{O:C}) \quad (1)$$
$$19$$

20 where M is the molar mass and O:C is the ratio of oxygen to carbon atoms. The coefficients
21 are: $A = -21.57 \text{ (K)}$, $B = 1.51 \text{ (K mol g}^{-1}\text{)}$, $C = -1.7 \times 10^{-3} \text{ (K mol}^2 \text{ g}^{-2}\text{)}$, $D = 131.4 \text{ (K)}$ and $E = -$
22 $0.25 \text{ (K mol g}^{-1}\text{)}$.

23 DeRieux et al. (2018) reported another parameterization (Eq. 2) to predict T_g of CH and CHO
24 compounds with molar mass up to $\sim 1100 \text{ g mol}^{-1}$ using the number of carbon (n_C), hydrogen
25 (n_H), and oxygen atoms (n_O):

$$26$$
$$27 T_g = (n_C^0 + \ln(n_C)) b_C + \ln(n_H) b_H + \ln(n_C) \ln(n_H) b_{CH} + \ln(n_O) b_O + \ln(n_C) \ln(n_O) b_{CO} \quad (2)$$
$$28$$

29 Values of the coefficients [n_C^0 , b_C , b_H , b_{CH} , b_O , and b_{CO}] are [1.96, 61.99, -113.33, 28.74, 0, 0]
30 for CH compounds and [12.13, 10.95, -41.82, 21.61, 118.96, -24.38] for CHO compounds
31 (DeRieux et al., 2018).

32 To estimate the T_g for a dry organic mixture ($T_{g,\text{org}}$), the relative mass concentration of each

1 compound was assumed to be proportional to its relative abundance in the mass spectrum and
2 the Gordon-Taylor mixing rule was employed with a Gordon-Taylor coefficient (k_{GT}) value of
3 1, as done previously for organic-organic mixtures (Dette et al., 2014).

4 For the T_g of a mixture of organics and water ($T_{g,mix}$), the effective hygroscopicity parameter
5 (κ) was applied to calculate the mass fraction of water in the SOA particles (Petters and
6 Kreidenweis, 2007). A κ value of 0.1 was used for the diesel fuel SOA based on an average
7 O:C of 0.45 for diesel fuel-derived SOA (Fig.S1 and Table S2 in Blair et al. (2017)) and the
8 relationship between O:C and κ reported in Lambe et al. (2011, Fig. 7) and Massoli et al. (2010,
9 Fig. 2). To estimate the $T_{g,mix}$, the Gordon-Taylor equation was applied with k_{GT} set to 2.5,
10 based on previous studies that suggested 2.5 ± 1.0 for organic-water mixtures (Zobrist et al.,
11 2008; Koop et al., 2011; Berkemeier et al., 2014).

12 Once $T_{g,mix}$ was determined, viscosity was estimated using the modified Vogel-Tammann-
13 Fulcher (VTF) equation and an assumed viscosity of 10^{12} Pa s at the glass transition
14 temperature ($T = T_g$) and an assumed viscosity of 10^{-5} Pa s at a very high temperature:

$$16 \log \eta = -5 + 0.434 \frac{T_0 D_f}{T - T_0} \quad (3)$$

$$17 \text{ where } T_0 = \frac{39.17 T_g}{D_f + 39.17} \quad (4)$$

18
19 The viscosity of 10^{-5} Pa s at a very high temperature is well established in the glass community
20 (Angell, 1991; Angell, 2002). In these equations, D_f is the fragility parameter and T_0 is the
21 Vogel temperature. In our calculations, we fixed D_f to be 10 because a previous study that
22 showed D_f approaches 10 when the molar mass of the organic compounds exceed ~ 200 g mol⁻¹
23 (DeRieux et al., 2018) and because many of the detected compounds in diesel SOA have
24 molar masses > 200 g mol⁻¹. Even though the D_f value does affect predicted viscosity (see Fig.
25 5b in DeRieux et al., 2018), D_f is not as critical as other parameters such as the glass transition
26 temperature or hygroscopicity.

28 **3 Results and discussion**

29 **3.1 LLPS in diesel fuel SOA**

30 Figures 1 and S2 show examples of images recorded during the LLPS experiments as the RH

1 was decreased from ~100% to ~0%. The five particles shown in Figs. 1 and S2 were produced
2 with the same reaction conditions. At the highest RH values (~100%), two phases were
3 observed in all cases. The inner phase was most likely a water-rich phase while the outer phase
4 was likely an organic-rich phase since the inner phase decreased in size as the RH decreased.
5 This conclusion is consistent with surface tensions of organics and experiments that have
6 investigated morphology of particles after LLPS (Jasper, 1972; Kwamena et al., 2010; Reid et
7 al., 2011; Song et al., 2013; O'Brien et al., 2015; Gorkowski et al., 2016, 2017). The organic-
8 rich phase was most likely non-crystalline since SOA contains thousands of molecules and the
9 concentration of any individual molecule is likely below the concentration required for
10 crystallization (Marcolli et al., 2004). At ~70 % RH, two liquid phases remained in all particles
11 (Figs. 1 and S2). Small amounts of the water-rich phase were present even at \lesssim 50 % RH in
12 most cases (Figs. 1 and S2). In the few cases where LLPS was not observed at \lesssim 50 %RH, two
13 liquid phases may still have been present in the particles, but not in the focus of the microscope.
14 In the previous studies using SOA derived from a single VOC, LLPS was observed when the
15 average O:C was between 0.34 and 0.44 but not when the average O:C was between 0.52 and
16 1.30 (Renbaum-Wolff et al., 2016; Rastak et al., 2017; Song et al., 2017). Consistent with this
17 trend, in the current studies, we observed LLPS when the O:C values of the SOA was 0.4 - 0.5
18 (Fig. S1b). However, in the previous studies using SOA derived from a single VOC, LLPS was
19 only observed between ~95 % and close to ~100 % RH. Whereas, in the current study, LLPS
20 was observed between ~70 % and close to ~100 %. This suggests that as the complexity of
21 SOA increases, LLPS can occur over a wider range of RH values. Consistent with this
22 conclusion, in a recent study, we showed that LLPS in organic particles containing two
23 commercially available organic compounds occurs over a wider RH range than in particles
24 containing only one organic compound (Song et al., 2018).

25 The increase in the range of RH values over which LLPS occurs is likely related to distribution
26 of the polarities (or hydrophilicities) of the organics molecules within the SOA (Renbaum-
27 Wolff et al., 2016; Gorkowski et al., 2019). When the organic molecules are hydrophobic or
28 moderately hydrophobic (and hence have small O:C values) the particles are expected to have
29 a single organic-rich phase until close to 100% RH, at which point LLPS can occur. When the
30 organic molecules are hydrophilic (and hence have large O:C values), the particles are expected
31 to have a single water-rich phase, with no occurrence of LLPS. Alternatively, if the particles

1 contain a mixture of hydrophobic and hydrophilic organic molecules, the particles are expected
2 to have both an organic-rich phase and a water-rich phase over a relatively wide range of RH
3 values. A significant amount of molecules with low and high O:C values in the diesel SOA
4 studied here (Fig. S3) is consistent with LLPS being observed over a relatively wide range of
5 RH values.

7 **3.2 Viscosity of diesel fuel-derived SOA**

8 **3.2.1 Lower limits to viscosity at 10% RH**

9 In these experiments, the RH was first decreased to 10% and particles were conditioned at this
10 RH for approximately 1 h. After conditioning, the particles were poked with a needle, which
11 caused the particles to crack (Fig. 2a). After poking, the sharp edges that resulted from cracking
12 moved by less than 0.5 μm in 5 h. The distance of 0.5 μm corresponds to the minimum amount
13 of movement that could be discerned in our microscope setup. Based on these results and fluid
14 dynamics simulations (Sect. S1 in the Supplement), the lower limit to the viscosity at 10 % RH
15 is 1×10^8 Pa s (Fig. 3a). This corresponds to roughly the viscosity of tar pitch (Koop et al., 2011).

16 **3.2.2. Lower limits to viscosity at 31 and 50 % RH**

17 In these experiments, the RH was first decreased to 31 % or 50 %, and conditioned at these RH
18 values for 1 h and 0.5 h, respectively. After conditioning the particles at either 31 or 50 % RH,
19 they were poked with a needle, resulting in the formation of a half-torus geometry (Figs. 2b
20 and 2c). From images recorded after poking the particles, the experimental flow time, $\tau_{exp, flow}$,
21 was determined, which corresponds to the time for the equivalent-area diameter of the inside
22 of the half torus geometry to reduce by 50 %. The equivalent-area diameter, d , was calculated
23 via the relationship $d = (4A/\pi)^{1/2}$ where A is the hole area (Reist, 1992). Based on the measured
24 $\tau_{exp, flow}$ values and fluid dynamics simulations (Renbaum-Wolff et al., 2013; Grayson et al.,
25 2015), and Sect. S2 in the Supplement, the lower limit to the viscosity is approximately 3×10^4
26 and 8×10^5 Pa s at 50 % and 31 % RH, respectively (Fig. 3a). For reference, the viscosity of
27 peanut butter corresponds is approximately 10^3 Pa s (Koop et al., 2011).

28 **3.2.3. Upper limits to viscosity at RH values ranging from 38 to 60 %**

29 In these experiments, the following new procedure was used. First, the particles were exposed
30 to a dry nitrogen flow at 0 % RH for ~ 1 h. After this exposure, the particles were poked with a
31 needle resulting in cracking of the particles. The RH above the particles was then increased in

1 a single step to one of the following RH values: 38 %, 41 %, 48 %, 53 %, 57 %, and 60 %. As
2 the RH increased and then stabilized (which took 5-10 min), the cracked particles began to
3 flow and returned to an approximately spherical cap shape (e.g. Fig. 4). From images recorded
4 during these experiments, the time required for the particles to return to a spherical cap shape
5 (starting from the cracked particles at RH= 0%) was determined. This time (which included
6 the time for the RH to increase and stabilize) was referred to as the experimental recovery time,
7 $\tau_{exp,recovery}$. Based on the $\tau_{exp,recovery}$ values and fluid dynamics simulations (Sect. S3 in the
8 Supplement), the upper limits of the viscosity is $\sim 1 \times 10^7$ Pa s and $\sim 1 \times 10^8$ Pa s at RH values of
9 60 % and 38 %, respectively (Fig. 3a).

10 **3.2.4 Comparison with previous measurements and predictions**

11 In Fig. 3b the measured viscosities determined from individual poke-and-flow experiments are
12 grouped by RH and compared with the viscosity of SOA generated by the photooxidation of
13 toluene. Toluene SOA is commonly used as a proxy of anthropogenic SOA (Pandis et al., 1992;
14 Robinson et al., 2013; Bateman et al., 2015; Liu et al., 2016; Song et al., 2016). The viscosities
15 of the toluene SOA and the diesel fuel SOA are similar. At RH values between 38 and 50 %
16 both have viscosities in the range of approximately 10^4 to 10^8 Pa s while at ≤ 10 % RH, both
17 have viscosities $\geq 1 \times 10^8$ Pa s.

18 In Fig. 3b, the viscosity of diesel fuel SOA is also compared with predicted viscosities based
19 on O:C and molar mass (Eq. 1) and the number of carbon, hydrogen, and oxygen atoms (Eq.
20 2). Within the uncertainty of the measurements, the predicted viscosities are consistent with
21 the measured viscosities (Fig. 3b). Measurements of viscosity with reduced uncertainties would
22 be useful to better test the predictions. Common methods used to measure viscosities (i.e., bulk
23 viscometers) are more precise than the poke-and-flow technique, but require more material
24 than is typically produced in environmental chambers (Reid et al., 2018).

25 Interestingly, predictions based on the number of carbon, hydrogen, and oxygen atoms (Eq. 2)
26 are almost 3 orders of magnitude higher than predictions based on O:C and molar mass (Eq. 1)
27 for dry conditions (i.e., 0 % RH) (Fig. 3b). Eq. 2 was applied to molar masses up to ~ 1100 g
28 mol^{-1} while Eq. 1 was applied to molar masses < 450 g mol^{-1} . If Eq. 2 was limited to molar
29 mass < 450 g mol^{-1} , the predicted viscosities would only decrease by a factor of ≤ 1.3 (Fig. S6).
30 The difference in the predictions based on Eq. 2 and Eq. 1 shown in Fig. 3b is due to the

1 uncertainties in those two parameterizations. More comprehensive experimental T_g datasets are
2 needed to further refine the T_g parameterizations.

3 The predicted viscosities shown in Fig. 3b only consider CH and CHO compounds. For the
4 diesel fuel SOA studied here, 257 compounds (~36% of the intensity weighted peaks) were
5 CHON compounds (Blair et al., 2017). A comprehensive experimental T_g dataset for organic
6 compounds containing nitrogen atoms is required to improve the viscosity predictions of diesel
7 fuel SOA.

8

9 **3.3 Diffusion coefficients and mixing times of large organics within diesel fuel SOA**

10 From the measured viscosities, we calculated diffusion coefficients of the organic molecules
11 within the diesel fuel SOA using the Stokes-Einstein relation:

12

$$13 \quad D_{org} = \frac{kT}{6\pi a\eta} \quad (5)$$

14

15 Where k is the Boltzmann constant, T is the temperature, a is the hydrodynamic radius of the
16 diffusing species, and η is the dynamic viscosity. To calculate diffusion coefficients, we
17 assumed a hydrodynamic radius of 0.4 nm for the diffusing organic molecules (Renbaum-Wolff
18 et al., 2013). Although the Stokes-Einstein relation may under predict diffusion of small
19 molecules (e.g., OH, O₃, NO_x, NH₃, and H₂O) in SOA, this equation gives reasonable values
20 when the size of the diffusing organics is similar to the size of the matrix molecules and the
21 temperature is not too close to the T_g of the matrix (Champion et al., 2000; Marshall et al., 2016;
22 Price et al., 2015, 2016; Bastelberger et al., 2017; Chenyakin et al., 2017; Ullmann et al., 2019).
23 Based on the measured viscosities and the Stokes-Einstein relation, the diffusion coefficients
24 of organics within Diesel SOA is $\leq 5.4 \times 10^{-17} \text{ cm}^2 \text{ s}^{-1}$ for RH values $\leq 10\%$ (Fig. 5a, secondary
25 y-axis). For RH values between 38 % and 50 %, the diffusion coefficients are in the range of
26 5.4×10^{-17} to $1.8 \times 10^{-13} \text{ cm}^2 \text{ s}^{-1}$.

27 From the calculated D_{org} , the mixing time of organics within 200 nm diesel fuel SOA particles,
28 τ_{mixing} , was calculated with the following equation (Seinfeld and Pandis, 2006; Shiraiwa et al.,
29 2011):

30

$$\tau_{mixing} = \frac{d^2}{4\pi D_{org}} \quad (6)$$

Where d corresponds to the diameter of the SOA particles. Values of τ_{mixing} represent the time after which the concentration of the diffusing molecules at the center of the particles deviates by less than e^{-1} from the equilibrium concentration. When calculating τ_{mixing} , we assumed d was 200 nm, which is consistent with the median diameter of the volume distribution of SOA in the atmosphere (Martin et al., 2010; Pöschl et al., 2010; Riipinen et al., 2011).

It is often assumed in chemical transport models that organic molecules are well mixed in SOA on the time scale of 1 h. Based on our viscosity results and Eq. 6, τ_{mixing} is ≥ 50 h at ≤ 10 % RH (Fig. 5a, secondary y-axis). This mixing time is much larger than assumed in chemical transport models. However, in the planetary boundary layer, the RH is not often ≤ 10 %, at least not when SOA concentrations are significant (Fig. 5b and 5c). Nevertheless, the large τ_{mixing} values at ≤ 10 % RH, may be important in laboratory experiments, where SOA is often generated and studied under low RH conditions on the time scales of minutes to hours. At 38 – 50 % RH τ_{mixing} are in the range ~ 0.01 h to ~ 50 h (Fig. 5a). These results provide important constraints on τ_{mixing} values within anthropogenic SOA.

Several caveats apply to the calculated τ_{mixing} values. First, the diesel fuel SOA was generated using relatively high particle mass concentrations ($\sim 500 \mu\text{g m}^{-3}$). The viscosity of diesel fuel SOA may be higher if generated using lower particle mass concentrations (Grayson et al., 2016; Jain et al., 2018). **Second, some of the semi-volatiles may have evaporated from the diesel fuel SOA in the poke-and-flow experiments. If evaporation of semi-volatiles did occur, the viscosity of the diesel fuel SOA at ($\sim 500 \mu\text{g m}^{-3}$) may be lower than reported here (Wilson et al., 2015; Yli-Juuti et al., 2017; Buchholz et al., 2019).** Third, τ_{mixing} values may be overestimated at low RH values due to the possible breakdown of the Stokes-Einstein relation near the glass transition RH (Champion et al., 2000; Bastelberger et al., 2017; Chenyakin et al., 2017; Evoy et al., 2019; Ullmann et al., 2019). Fourth, when calculating the viscosity, we did not take into account the heterogeneity of the particle (i.e. the presence of both an organic-rich and water-rich phase). The viscosity measurements were carried out at RH values $\lesssim 58$ % RH. For this RH range, the amount of the water-rich phase was small but still detectable in most cases. Assuming the water-rich phase is less viscous than the organic-rich phase, due to the

1 plasticizing effect of water, the viscosity of the organic-rich phase will be greater than the
2 calculated (i.e. reported) viscosities.

4 **4 Summary and conclusions**

5 We investigated LLPS in SOA generated from diesel fuel vapors. Diesel fuel contains a wide
6 range of VOCs, and diesel fuel SOA may be a reasonable proxy for SOA from anthropogenic
7 emissions. Two liquid phases (an organic-rich outer phase and a water-rich inner phase) were
8 observed in the diesel fuel SOA at RH values ranging from ~70 % to ~100 %. These results
9 may be important for predicting the cloud nucleating ability of anthropogenic SOA since the
10 presence of an organic-rich outer phase at high RH values can lower the supersaturation with
11 respect to water required for cloud droplet formation (Petters et al. 2006; Hodas et al. 2016;
12 Renbaum-Wolff et al., 2016; Rastak et al., 2017; Ovadnevaite et al., 2017; Liu et al., 2018).
13 The presence of two liquid phases at RH values as low as ~70 % may also impact heterogeneous
14 chemistry, growth, and optical properties of SOA (Zuend et al., 2010; Zuend and Seinfeld, 2012;
15 Shiraiwa et al., 2013b; Freedman, 2017; Fard et al., 2018; Zhang et al., 2018). We conclude
16 that LLPS should be considered when predicting the cloud nucleating ability, reactivity, growth,
17 and optical properties of SOA from anthropogenic emissions.

18 We also investigated the viscosity of diesel fuel SOA using the poke-and-flow technique
19 together with simulations of fluid flow. For RH values of ≤ 10 %, the viscosity was $\geq 1 \times 10^8$ Pa
20 s. At RH values between 30 and 50 % the viscosity was in the range of 1×10^8 to 3×10^4 Pa s.
21 The measured viscosities were consistent with predictions based on molar mass and O:C and
22 predictions based on the number of carbon, hydrogen, and oxygen atoms of identified SOA
23 compounds. Additional measurements of viscosity of diesel fuel SOA with reduced
24 uncertainties would be useful to better test the predictions. Furthermore, additional
25 comprehensive experimental T_g datasets are needed to further refine the parameterizations.

26 Based on these measured viscosities and the Stokes-Einstein relation, diffusion coefficients and
27 τ_{mixing} values of organics within diesel fuel SOA particles were calculated. For RH values \leq
28 10%, diffusion coefficients are $\leq 5.4 \times 10^{-17}$ cm² s⁻¹ and τ_{mixing} is ≥ 50 h. Such low RH values
29 are not common in the planetary boundary layer, but are common in laboratory experiments
30 when generating SOA. We conclude that these large τ_{mixing} should be considered when
31 interpreting laboratory data of SOA generated under low RH conditions. For RH values

1 between 38 % and 50 %, the diffusion coefficients are in the range of 5.4×10^{-17} to 1.8×10^{-13}
2 $\text{cm}^2 \text{s}^{-1}$ and τ_{mixing} values are in the range of ~ 0.01 h and ~ 50 h. These results provide important
3 constraints on diffusion coefficients and τ_{mixing} values within anthropogenic SOA. Further
4 studies are needed using more atmospherically relevant mass concentrations since a relatively
5 high mass concentration ($\sim 500 \mu\text{g m}^{-3}$) of the SOA was used when generating the SOA in this
6 work.

8 **Conflicts of interest**

9 There are no conflicts of interest to declare.

11 **Author contributions**

12 A.K.B designed the study. M.Song, A.M.M, and Y. H. performed the viscosity and LLPS
13 experiments. S.A.N., N.R.S., S.L.B., J. L., and A.L. generated the SOA samples and analyzed
14 their chemical compositions. W.-S.W.D., Y.L., and M.S. predicted viscosities. M.Song and
15 A.K.B. prepared the manuscript with contributions from all co-authors.

17 **Acknowledgements**

18 This work was supported by the Natural Sciences and Engineering Research Council of Canada.
19 M. Song acknowledges funding from the National Research Foundation of Korea (NRF), the
20 Korea Government (MSIP) (2016R1C1B1009243) and Korea Institute of Toxicology (KIT)
21 (KK-1905-02). M.S. acknowledges funding from the U.S. National Science Foundation (AGS-
22 1654104) and the U.S. Department of Energy (DE-SC0018349). The AMS instrument used in
23 this work was acquired with the NSF grant MRI-0923323.

25 **References**

- 26 Abramson, E., Imre, D., Beranek, J., Wilson, J., and Zelenyuk, A.: Experimental determination
27 of chemical diffusion within secondary organic aerosol particles, *Phys. Chem. Chem.*
28 *Phys.*, 15, 2983-2991, <https://doi.10.1039/C2cp44013j>, 2013.
- 29 Altaft, M. B., Dutcher, D. D., Raymond, T. M., and Freedman, M. A.: Effect of Particle
30 Morphology on Cloud Condensation Nuclei Activity, *ACS. Earth Space Chem.*, 2, 634-
31 639, [10.1021/acsearthspacechem.7b00146](https://doi.10.1021/acsearthspacechem.7b00146), 2018.
- 32 Angell, C. A.: Relaxation in liquids, Polymers and plastic crystals - Strong fragile patterns and

1 problems, *J. Non-Cryst. Solids*, 131, 13-31, [https://doi.10.1016/0022-3093\(91\)90266-9](https://doi.10.1016/0022-3093(91)90266-9),
2 1991.

3 Angell, C. A.: Liquid fragility and the glass transition in water and aqueous solutions, *Chem.*
4 *Rev.*, 102, 2627-2649, UNSP CR000689Q 10.1021/cr000689q, 2002.

5 Baltensperger, U., Dommen, J., Alfarra, R., Duplissy, J., Gaeggeler, K., Metzger, A., Facchini,
6 M. C., Decesari, S., Finessi, E., Reinnig, C., Schott, M., Warnke, J., Hoffmann, T., Klatzer,
7 B., Puxbaum, H., Geiser, M., Savi, M., Lang, D., Kalberer, M., and Geiser, T.: Combined
8 determination of the chemical composition and of health effects of secondary organic
9 aerosols: The POLYSOA project, *J Aerosol Med Pulm D*, 21, 145-154, 2008.

10 Bastelberger, S., Krieger, U. K., Luo, B. P., and Peter, T.: Diffusivity measurements of volatile
11 organics in levitated viscous aerosol particles, *Atmos. Chem. Phys.*, 17, 8453-8471,
12 10.5194/acp-17-8453-2017, 2017.

13 Bateman, A. P., Bertram, A. K., and Martin, S. T.: Hygroscopic influence on the semisolid-to-
14 liquid transition of secondary organic materials, *J. Phys. Chem. A.*, 119, 4386-4395,
15 10.1021/jp508521c, 2015.

16 Berkemeier, T., Shiraiwa, M., Pöschl, U., and Koop, T.: Competition between water uptake and
17 ice nucleation by glassy organic aerosol particles, *Atmos. Chem. Phys.*, 14, 12513-12531,
18 2014.

19 Bertram, A. K., Martin, S. T., Hanna, S. J., Smith, M. L., Bodsworth, A., Chen, Q., Kuwata,
20 M., Liu, A., You, Y., and Zorn, S. R.: Predicting the relative humidities of LLPS,
21 efflorescence, and deliquescence of mixed particles of ammonium sulfate, organic material,
22 and water using the organic-to-sulfate mass ratio of the particle and the oxygen-to-carbon
23 elemental ratio of the organic component, *Atmos. Chem. Phys.*, 11, 10995-11006,
24 <https://doi.10.5194/acp-11-10995-2011>, 2011.

25 Blair, S. L., MacMillan, A. C., Drozd, G. T., Goldstein, A. H., Chu, R. K., Pasa-Tolic, L., Shaw,
26 J. B., Tolic, N., Lin, P., Laskin, J., Laskin, A., and Nizkorodov, S. A.: Molecular
27 characterization of organosulfur compounds in biodiesel and diesel fuel secondary organic
28 aerosol, *Environ. Sci. Technol.*, 51, 119-127, 10.1021/acs.est.6b03304, 2017.

29 Bodsworth, A., Zobrist, B., and Bertram, A. K.: Inhibition of efflorescence in mixed organic-
30 inorganic particles at temperatures less than 250K, *Phys. Chem. Chem. Phys.*, 12, 15144-
31 15144, 2010.

32 **Buchholz, A., Lambe, A. T., Ylisirio, A., Li, Z. J., Tikkanen, O. P., Faiola, C., Kari, E., Hao,**

1 L. Q., Luoma, O., Huang, W., Mohr, C., Worsnop, D. R., Nizkorodov, S. A., Yli-Juuti, T.,
2 Schobesberger, S., and Virtanen, A.: Insights into the O : C-dependent mechanisms
3 controlling the evaporation of alpha-pinene secondary organic aerosol particles, *Atmos.*
4 *Chem. Phys.*, 19, 4061-4073, 10.5194/acp-19-4061-2019, 2019.

5 Canagaratna, M. R., Jimenez, J. L., Kroll, J. H., Chen, Q., Kessler, S. H., Massoli, P.,
6 Hildebrandt Ruiz, L., Fortner, E., Williams, L. R., Wilson, K. R., Surratt, J. D., Donahue,
7 N. M., Jayne, J. T., and Worsnop, D. R.: Elemental ratio measurements of organic
8 compounds using aerosol mass spectrometry: characterization, improved calibration, and
9 implications, *Atmos. Chem. Phys.*, 15, 253-272, 10.5194/acp-15-253-2015, 2015.

10 Cappa, C. D., and Wilson, K. R.: Evolution of organic aerosol mass spectra upon heating:
11 implications for OA phase and partitioning behavior, *Atmos. Chem. Phys.*, 11, 1895-1911,
12 <https://doi.10.5194/acp-11-1895-2011>, 2011.

13 Champion, D., Le Meste, M., and Simatos, D.: Towards an improved understanding of glass
14 transition and relaxations in foods: molecular mobility in the glass transition range, *Trends*
15 *Food Sci. Tech.*, 11, 41-55, [https://doi.10.1016/S0924-2244\(00\)00047-9](https://doi.10.1016/S0924-2244(00)00047-9), 2000.

16 Chenyakin, Y., Ullmann, D. A., Evoy, E., Renbaum-Wolff, L., Kamal, S., and Bertram, A. K.:
17 Diffusion coefficients of organic molecules in sucrose-water solutions and comparison
18 with Stokes-Einstein predictions, *Atmos. Chem. Phys.*, 17, 2423-2435, 10.5194/acp-17-
19 2423-2017, 2017.

20 Ciobanu, V. G., Marcolli, C., Krieger, U. K., Weers, U., and Peter, T.: Liquid-Liquid Phase
21 Separation in Mixed Organic/Inorganic Aerosol Particles, *J. Phys. Chem. A*, 113, 10966–
22 10978, <https://doi.org/10.1021/Jp905054d>, 2009.

23 Davies, J. F., Zuend, A., and Wilson, K. R.: Technical note: The role of evolving surface tension
24 in the formation of cloud droplets, *Atmos. Chem. Phys.*, 19, 2933-2946, 10.5194/acp-19-
25 2933-2019, 2019.

26 de Gouw, J. A., Brock, C. A., Atlas, E. L., Bates, T. S., Fehsenfeld, F. C., Goldan, P. D.,
27 Holloway, J. S., Kuster, W. C., Lerner, B. M., Matthew, B. M., Middlebrook, A. M.,
28 Onasch, T. B., Peltier, R. E., Quinn, P. K., Senff, C. J., Stohl, A., Sullivan, A. P., Trainer,
29 M., Warneke, C., Weber, R. J., and Williams, E. J.: Sources of particulate matter in the
30 northeastern United States in summer: 1. Direct emissions and secondary formation of
31 organic matter in urban plumes, *J. Geophys. Res.-Atmos.*, 113, D08301,
32 <https://doi.10.1029/2007jd009243>, 2008.

1 Dette, H. P., Qi, M. A., Schroder, D. C., Godt, A., and Koop, T.: Glass-forming properties of 3-
2 methylbutane-1,2,3-tricarboxylic acid and its mixtures with water and pinonic acid, *J. Phys.*
3 *Chem. A*, 118, 7024-7033, 10.1021/jp505910w, 2014.

4 DeRieux, W. S., Li, Y., Lin, P., Laskin, J., Laskin, A., Bertram, A. K., Nizkorodov, S. A., and
5 Shiraiwa, M.: Predicting the glass transition temperature and viscosity of secondary
6 organic material using molecular composition, *Atmos. Chem. Phys.*, 18, 6331-6351,
7 10.5194/acp-18-6331-2018, 2018.

8 Ervens, B., Turpin, B. J., and Weber, R. J.: Secondary organic aerosol formation in cloud
9 droplets and aqueous particles (aqSOA): a review of laboratory, field and model studies,
10 *Atmos. Chem. Phys.*, 11, 11069-11102, DOI 10.5194/acp-11-11069-2011, 2011.

11 Evoy, E., Maclean, A. M., Rovelli, G., Li, Y., Tsimpidi, A. P., Karydis, V. A., Kamal, S.,
12 Lelieveld, J., Shiraiwa, M., Reid, J. P., and Bertram, A. K.: Predictions of diffusion rates
13 of organic molecules in secondary organic aerosols using the Stokes-Einstein and
14 fractional Stokes-Einstein relations, *Atmos. Chem. Phys. Discuss.*,
15 <https://doi.org/10.5194/acp-2019-191>, in review, 2019.

16 Fard, M. M., Krieger, U. K., and Peter, T.: Shortwave radiative impact of liquid-liquid phase
17 separation in brown carbon aerosols, *Atmos. Chem. Phys.*, 18, 13511-13530, 10.5194/acp-
18 18-13511-2018, 2018.

19 Freedman, M. A.: Phase separation in organic aerosol, *Chem. Soc. Rev.*, 46, 7694-7705,
20 10.1039/c6cs00783j, 2017.

21 Gentner, D. R., Isaacman, G., Worton, D. R., Chan, A. W. H., Dallmann, T. R., Davis, L., Liu,
22 S., Day, D. A., Russell, L. M., Wilson, K. R., Weber, R., Guha, A., Harley, R. A., and
23 Goldstein, A. H.: Elucidating secondary organic aerosol from diesel and gasoline vehicles
24 through detailed characterization of organic carbon emissions, *Proc. Natl. Acad. Sci. US*,
25 109, 18318-18323, 10.1073/pnas.1212272109, 2012.

26 Gentner, D. R., Jathar, S. H., Gordon, T. D., Bahreini, R., Day, D. A., El Haddad, I., Hayes, P.
27 L., Pieber, S. M., Platt, S. M., de Gouw, J., Goldstein, A. H., Harley, R. A., Jimenez, J. L.,
28 Prevot, A. S. H., and Robinson, A. L.: Review of Urban Secondary Organic Aerosol
29 Formation from Gasoline and Diesel Motor Vehicle Emissions, *Environ Sci Technol*, 51,
30 1074-1093, 2017.

31 Gorkowski, K., Beydoun, H., Aboff, M., Walker, J. S., Reid, J. P., and Sullivan, R. C.:
32 Advanced aerosol optical tweezers chamber design to facilitate phase-separation and

1 equilibration timescale experiments on complex droplets, *Aerosol. Sci. Tech.*, 50, 1327–
2 1341, <https://doi.org/10.1080/02786826.2016.1224317>, 2016.

3 Gorkowski, K., Donahue, N. M., and Sullivan, R. C.: Emulsified and Liquid Liquid Phase-
4 Separated States of alphaPinene Secondary Organic Aerosol Determined Using Aerosol
5 Optical Tweezers, *Environ. Sci. Technol.*, 51, 12154–12163,
6 <https://doi.org/10.1021/acs.est.7b03250>, 2017.

7 Gorkowski, K., Preston, T. C., and Zuend, A.: RH-dependent organic aerosol thermodynamics
8 via an efficient reduced-complexity model, *Atmos. Chem. Phys. Discuss.*,
9 <https://doi.org/10.5194/acp-2019-495>, in review, 2019.

10 Grayson, J. W., Song, M., Sellier, M., and Bertram, A. K.: Validation of the poke-flow
11 technique combined with simulations of fluid flow for determining viscosities in samples
12 with small volumes and high viscosities, *Atmos. Meas. Tech.*, 8, 2463-2472, 2015.

13 Grayson, J. W., Zhang, Y., Mutzel, A., Renbaum-Wolff, L., Boge, O., Kamal, S., Herrmann, H.,
14 Martin, S. T., and Bertram, A. K.: Effect of varying experimental conditions on the
15 viscosity of alpha-pinene derived secondary organic material, *Atmos. Chem. Phys.*, 16,
16 6027-6040, [10.5194/acp-16-6027-2016](https://doi.org/10.5194/acp-16-6027-2016), 2016.

17 Grayson, J. W., Evoy, E., Song, M., Chu, Y. X., Maclean, A., Nguyen, A., Upshur, M. A.,
18 Ebrahimi, M., Chan, C. K., Geiger, F. M., Thomson, R. J., and Bertram, A. K.: The effect
19 of hydroxyl functional groups and molar mass on the viscosity of non-crystalline organic
20 and organic-water particles, *Atmos. Chem. Phys.*, 17, 8509-8524, [10.5194/acp-17-8509-](https://doi.org/10.5194/acp-17-8509-2017)
21 2017, 2017.

22 Hallquist, M., Wenger, J. C., Baltensperger, U., Rudich, Y., Simpson, D., Claeys, M., Dommen,
23 J., Donahue, N. M., George, C., Goldstein, A. H., Hamilton, J. F., Herrmann, H., Hoffmann,
24 T., Iinuma, Y., Jang, M., Jenkin, M. E., Jimenez, J. L., Kiendler-Scharr, A., Maenhaut, W.,
25 McFiggans, G., Mentel, T. F., Monod, A., Prevot, A. S. H., Seinfeld, J. H., Surratt, J. D.,
26 Szmigielski, R., and Wildt, J.: The formation, properties and impact of secondary organic
27 aerosol: current and emerging issues, *Atmos. Chem. Phys.*, 9, 5155-5236, 2009.

28 Ham, S., Babar, Z. B., Lee, J. B., Lim, H.-J., and Song, M.: Liquid–liquid phase separation in
29 secondary organic aerosol particles produced from α -pinene ozonolysis and α -pinene
30 photooxidation with/without ammonia, *Atmos. Chem. Phys.*, 19, 9321-9331,
31 <https://doi.org/10.5194/acp-19-9321-2019>, 2019.

32 Hayes, P. L., Carlton, A. G., Baker, K. R., Ahmadov, R., Washenfelder, R. A., Alvarez, S.,

1 Rappengluck, B., Gilman, J. B., Kuster, W. C., de Gouw, J. A., Zotter, P., Prevot, A. S. H.,
2 Szidat, S., Kleindienst, T. E., Offenberg, J. H., Ma, P. K., and Jimenez, J. L.: Modeling the
3 formation and aging of secondary organic aerosols in Los Angeles during CalNex 2010,
4 *Atmos. Chem. Phys.*, 15, 5773-5801, 10.5194/acp-15-5773-2015, 2015.

5 Hodas, N., Zuend, A., Schilling, K., Berkemeier, T., Shiraiwa, M., Flagan, R. C., and Seinfeld,
6 J. H.: Discontinuities in hygroscopic growth below and above water saturation for
7 laboratory surrogates of oligomers in organic atmospheric aerosols, *Atmos. Chem. Phys.*,
8 16, 12767-12792, 10.5194/acp-16-12767-2016, 2016.

9 Houle, F. A., Hinsberg, W. D., and Wilson, K. R.: Oxidation of a model alkane aerosol by OH
10 radical: the emergent nature of reactive uptake, *Phys. Chem. Chem. Phys.*, 17, 4412-4423,
11 2015.

12 IPCC: Climate Change 2013: The Physical science basis. Contribution of working group I to
13 the fifth assessment report of the intergovernmental panel on climate change, edited by:
14 Stocker, T. F., Qin, D., Plattner, G.-K., Tignor, M., Allen, S. K., Boschung, J., Nauels, A.,
15 Xia, Y., Bex, V., and Midgley, P. M., Cambridge University Press, Cambridge, UK and
16 New York, NY, US, 1535, 2013.

17 Jain, S., Fischer, K. B., and Petrucci, G. A.: The Influence of absolute mass loading of
18 secondary organic aerosols on their phase state, *Atmosphere-Basel*, 9, ARTN 131
19 10.3390/atmos9040131, 2018.

20 Jang, M., Ghio, A. J., and Cao, G.: Exposure of BEAS-2B cells to secondary organic aerosol
21 coated on magnetic nanoparticles, *Chem. Res. Toxicol.*, 19, 1044-1050, 2006.

22 Jasper, J. J.: The surface tension of pure liquid compounds, *J. Phys. Chem. Ref. Data*, 1, 841–
23 1009, <https://doi.org/10.1063/1.3253106>, 1972.

24 Jathar, S. H., Miracolo, M. A., Tkacik, D. S., Donahue, N. M., Adams, P. J., and Robinson, A.
25 L.: Secondary organic aerosol formation from photo-oxidation of unburned fuel:
26 Experimental results and implications for aerosol formation from combustion emissions,
27 *Environ. Sci. Technol.*, 47, 12886-12893, 2013.

28 Jathar, S. H., Donahue, N. M., Adams, P. J., and Robinson, A. L.: Testing secondary organic
29 aerosol models using smog chamber data for complex precursor mixtures: influence of
30 precursor volatility and molecular structure, *Atmos. Chem. Phys.*, 14, 5771-5780, 2014.

31 Jathar, S. H., Heppding, C., Link, M. F., Farmer, D. K., Akherati, A., Kleeman, M. J., de Gouw,
32 J. A., Veres, P. R., and Roberts, J. M.: Investigating diesel engines as an atmospheric source

1 of isocyanic acid in urban areas, *Atmos. Chem. Phys.*, 17, 8959-8970, 2017.

2 Ji, Z. R., Zhang, Y., Pang, S. F., and Zhang, Y. H.: Crystal nucleation and crystal growth and
3 mass transfer in internally mixed sucrose/NaNO₃ particles, *J. Phys. Chem. A*, 121, 7968-
4 7975, 10.1021/acs.jpca.7b08004, 2017.

5 Jimenez, J. L., Canagaratna, M. R., Donahue, N. M., Prevot, A. S. H., Zhang, Q., Kroll, J. H.,
6 DeCarlo, P. F., Allan, J. D., Coe, H., Ng, N. L., Aiken, A. C., Docherty, K. S., Ulbrich, I.
7 M., Grieshop, A. P., Robinson, A. L., Duplissy, J., Smith, J. D., Wilson, K. R., Lanz, V. A.,
8 Hueglin, C., Sun, Y. L., Tian, J., Laaksonen, A., Raatikainen, T., Rautiainen, J., Vaattovaara,
9 P., Ehn, M., Kulmala, M., Tomlinson, J. M., Collins, D. R., Cubison, M. J., Dunlea, E. J.,
10 Huffman, J. A., Onasch, T. B., Alfarra, M. R., Williams, P. I., Bower, K., Kondo, Y.,
11 Schneider, J., Drewnick, F., Borrmann, S., Weimer, S., Demerjian, K., Salcedo, D., Cottrell,
12 L., Griffin, R., Takami, A., Miyoshi, T., Hatakeyama, S., Shimono, A., Sun, J. Y., Zhang,
13 Y. M., Dzepina, K., Kimmel, J. R., Sueper, D., Jayne, J. T., Herndon, S. C., Trimborn, A.
14 M., Williams, L. R., Wood, E. C., Middlebrook, A. M., Kolb, C. E., Baltensperger, U., and
15 Worsnop, D. R.: Evolution of organic aerosols in the atmosphere, *Science*, 326, 1525-1529,
16 <https://doi.10.1126/science.1180353>, 2009.

17 Kanakidou, M., Seinfeld, J. H., Pandis, S. N., Barnes, I., Dentener, F. J., Facchini, M. C., Van
18 Dingenen, R., Ervens, B., Nenes, A., Nielsen, C. J., Swietlicki, E., Putaud, J. P., Balkanski,
19 Y., Fuzzi, S., Horth, J., Moortgat, G. K., Winterhalter, R., Myhre, C. E. L., Tsigaridis, K.,
20 Vignati, E., Stephanou, E. G., and Wilson, J.: Organic aerosol and global climate
21 modelling: a review, *Atmos. Chem. Phys.*, 5, 1053-1123, 2005.

22 Kidd, C., Perraud, V., Wingen, L. M., and Finlayson-Pitts, B. J.: Integrating phase and
23 composition of secondary organic aerosol from the ozonolysis of alpha-pinene, *P. Natl.*
24 *Acad. Sci. USA*, 111, 7552-7557, <https://doi.10.1073/pnas.1322558111>, 2014.

25 Kim, Y., Sartelet, K., and Couvidat, F.: Modeling the effect of non-ideality, dynamic mass
26 transfer and viscosity on SOA formation in a 3-D air quality model, *Atmos. Chem. Phys.*,
27 19, 1241-1261, 10.5194/acp-19-1241-2019, 2019.

28 Knopf, D. A.: Thermodynamic properties and nucleation processes of upper tropospheric and
29 lower stratospheric aerosol particles, Diss. ETH No. 15103, Zurich, Switzerland, 2003.

30 Knopf, D. A., Alpert, P. A., and Wang, B. B.: The Role of Organic Aerosol in Atmospheric Ice
31 Nucleation: A Review, *Ac. Earth Space Chem.*, 2, 168-202,
32 10.1021/acsearthspacechem.7b00120, 2018.

- 1 Koop, T., Bookhold, J., Shiraiwa, M., and Poschl, U.: Glass transition and phase state of organic
2 compounds: dependency on molecular properties and implications for secondary organic
3 aerosols in the atmosphere, *Phys. Chem. Chem. Phys.*, 13, 19238-19255,
4 <https://doi.10.1039/C1cp22617g>, 2011.
- 5 Krieger, U. K., Marcolli, C., and Reid, J. P.: Exploring the complexity of aerosol particle
6 properties and processes using single particle techniques, *Chem. Soc. Rev.*, 41, 6631–6662,
7 <https://doi.org/10.1039/c2cs35082c>, 2012.
- 8 Kuwata, M., and Martin, S. T.: Phase of atmospheric secondary organic material affects its
9 reactivity, *P. Natl. Acad. Sci. USA*, 109, 17354-17359, 2012.
- 10 Kwamena, N. O. A., Buajareern, J., and Reid, J. P.: Equilibrium Morphology of Mixed
11 Organic/Inorganic/Aqueous Aerosol Droplets: Investigating the effect of RH and
12 surfactants, *J. Phys. Chem. A*, 114, 5787–5795, <https://doi.org/10.1021/Jp1003648>, 2010.
- 13 Ladino, L. A., Zhou, S., Yakobi-Hancock, J. D., Aljawhary, D., and Abbatt, J. P. D.: Factors
14 controlling the ice nucleating abilities of alpha-pinene SOA particles, *J. Geophys. Res.-*
15 *Atmos.*, 119, 9041-9051, 2014.
- 16 Lambe, A. T., Onasch, T. B., Massoli, P., Croasdale, D. R., Wright, J. P., Ahern, A. T.,
17 Williams, L. R., Worsnop, D. R., Brune, W. H., and Davidovits, P.: Laboratory studies of
18 the chemical composition and cloud condensation nuclei (CCN) activity of secondary
19 organic aerosol (SOA) and oxidized primary organic aerosol (OPOA), *Atmos. Chem.*
20 *Phys.*, 11, 8913-8928, DOI 10.5194/acp-11-8913-2011, 2011.
- 21 Li, Y. J., Liu, P., Gong, Z., Wang, Y., Bateman, A. P., Bergoend, C., Bertram, A. K., and Martin,
22 S. T.: Chemical reactivity and liquid/nonliquid states of secondary organic material,
23 *Environ. Sci. and Tech.*, 49, 13264-13274, [10.1021/acs.est.5b03392](https://doi.org/10.1021/acs.est.5b03392), 2015.
- 24 Li, Z. Y., Smith, K. A., and Cappa, C. D.: Influence of relative humidity on the heterogeneous
25 oxidation of secondary organic aerosol, *Atmos. Chem. Phys.*, 18, 14585-14608,
26 [10.5194/acp-18-14585-2018](https://doi.org/10.5194/acp-18-14585-2018), 2018.
- 27 Liu, S., Ahlm, L., Day, D. A., Russell, L. M., Zhao, Y. L., Gentner, D. R., Weber, R. J.,
28 Goldstein, A. H., Jaoui, M., Offenberg, J. H., Kleindienst, T. E., Rubitschun, C., Surratt, J.
29 D., Sheesley, R. J., and Scheller, S.: Secondary organic aerosol formation from fossil fuel
30 sources contribute majority of summertime organic mass at Bakersfield, *J. Geophys. Res.-*
31 *Atmos.*, 117, 2012.
- 32 Liu, P. F., Li, Y. J., Wang, Y., Gilles, M. K., Zaveri, R. A., Bertram, A. K., and Martin, S. T.:

1 Lability of secondary organic particulate matter, *P. Natl. Acad. Sci. US*, 113, 12643-12648,
2 10.1073/pnas.1603138113, 2016.

3 Liu, P., Song, M., Zhao, T., Gunthe, S. S., Ham, S., He, Y., Qin, Y. M., Gong, Z., Amorim, J.
4 C., Bertram, A. K., and Martin, S. T.: Resolving the mechanisms of hygroscopic growth
5 and cloud condensation nuclei activity for organic particulate matter, *Nat. Commun.*, 9,
6 4076, 10.1038/s41467-018-06622-2, 2018.

7 Loza, C. L., Coggon, M. M., Nguyen, T. B., Zuend, A., Flagan, R. C., and Seinfeld, J. H.: On
8 the mixing and evaporation of secondary organic aerosol components, *Environ. Sci.*
9 *Technol.*, 47, 6173-6180, 10.1021/es400979k, 2013.

10 Maclean, A. M., Butenhoff, C. L., Grayson, J. W., Barsanti, K., Jimenez, J. L., and Bertram, A.
11 K.: Mixing times of organic molecules within secondary organic aerosol particles: a global
12 planetary boundary layer perspective, *Atmos. Chem. Phys.*, 17, 13037-13048,
13 10.5194/acp-17-13037-2017, 2017.

14 Marcolli, C., Luo, B., Peter, T.: Mixing of the organic aerosol fractions: Liquids as the
15 thermodynamically stable phases, *J. Phys. Chem. A*, 108, 2216-2224, 10.1021/jp036080l,
16 2004.

17 Marcolli, C. and Krieger, U. K.: Phase changes during hygroscopic cycles of mixed
18 organic/inorganic model systems of tropospheric aerosols, *J. Phys. Chem. A*, 110, 1881–
19 1893, <https://doi.org/10.1021/Jp0556759>, 2006.

20 Marshall, F. H., Miles, R. E. H., Song, Y. C., Ohm, P. B., Power, R. M., Reid, J. P., and Dutcher,
21 C. S.: Diffusion and reactivity in ultraviscous aerosol and the correlation with particle
22 viscosity, *Chem. Sci.*, 7, 1298-1308, 10.1039/c5sc03223g, 2016.

23 Martin, S. T., Andreae, M. O., Althausen, D., Artaxo, P., Baars, H., Borrmann, S., Chen, Q.,
24 Farmer, D. K., Guenther, A., Gunthe, S. S., Jimenez, J. L., Karl, T., Longo, K., Manzi, A.,
25 Müller, T., Pauliquevis, T., Petters, M. D., Prenni, A. J., Pöschl, U., Rizzo, L. V., Schneider,
26 J., Smith, J. N., Swietlicki, E., Tota, J., Wang, J., Wiedensohler, A., and Zorn, S. R.: An
27 overview of the Amazonian aerosol characterization experiment 2008 (AMAZE-08),
28 *Atmos. Chem. Phys.*, 10, 11415–11438, <https://doi.org/10.5194/acp-10-11415-2010>, 2010.

29 Massoli, P., Lambe, A. T., Ahern, A. T., Williams, L. R., Ehn, M., Mikkila, J., Canagaratna, M.
30 R., Brune, W. H., Onasch, T. B., Jayne, J. T., Petaja, T., Kulmala, M., Laaksonen, A., Kolb,
31 C. E., Davidovits, P., and Worsnop, D. R.: Relationship between aerosol oxidation level
32 and hygroscopic properties of laboratory generated secondary organic aerosol (SOA)

1 particles, *Geophys. Res. Lett.*, 37, Artn L24801, 10.1029/2010gl045258, 2010.

2 Mu, Q., Shiraiwa, M., Octaviani, M., Ma, N., Ding, A. J., Su, H., Lammel, G., Poschl, U., and
3 Cheng, Y. F.: Temperature effect on phase state and reactivity controls atmospheric
4 multiphase chemistry and transport of PAHs, *Sci. Adv.*, 4, UNSP eaap7314
5 10.1126/sciadv.aap7314, 2018.

6 Murray, B. J.: Inhibition of ice crystallisation in highly viscous aqueous organic acid droplets,
7 *Atmos. Chem. Phys.*, 8, 5423-5433, 2008.

8 Murray, B. J., and Bertram, A. K.: Inhibition of solute crystallisation in aqueous H^+ - NH_4^+ -
9 SO_4^{2-} - H_2O droplets, *Phys. Chem. Chem. Phys.*, 10, 3287-3301, 2008.

10 Murray, B. J., Wilson, T. W., Dobbie, S., Cui, Z. Q., Al-Jumur, S. M. R. K., Mohler, O.,
11 Schnaiter, M., Wagner, R., Benz, S., Niemand, M., Saathoff, H., Ebert, V., Wagner, S., and
12 Karcher, B.: Heterogeneous nucleation of ice particles on glassy aerosols under cirrus
13 conditions, *Nat. Geosci.*, 3, 233-237, <https://doi.10.1038/Ngeo817>, 2010.

14 Murray, B. J., Haddrell, A. E., Peppe, S., Davies, J. F., Reid, J. P., O'Sullivan, D., Price, H. C.,
15 Kumar, R., Saunders, R. W., Plane, J. M. C., Umo, N. S., and Wilson, T. W.: Glass
16 formation and unusual hygroscopic growth of iodic acid solution droplets with relevance
17 for iodine mediated particle formation in the marine boundary layer, *Atmos. Chem. Phys.*,
18 12, 8575-8587, <https://doi.10.5194/acp-12-8575-2012>, 2012.

19 O'Brien, R. E., Wang, B. B., Kelly, S. T., Lundt, N., You, Y., Bertram, A. K., Leone, S. R.,
20 Laskin, A., and Gilles, M. K.: Liquid-Liquid Phase Separation in Aerosol Particles:
21 Imaging at the Nanometer Scale, *Environ. Sci. Technol.*, 49, 4995–5002,
22 <https://doi.org/10.1021/acs.est.5b00062>, 2015.

23 Odum, J. R., Jungkamp, T. P. W., Griffin, R. J., Flagan, R. C., and Seinfeld, J. H.: The
24 atmospheric aerosol-forming potential of whole gasoline vapor, *Science*, 276, 96-99,
25 <https://doi.10.1126/science.276.5309.96>, 1997.

26 Ovadnevaite, J., Zuend, A., Laaksonen, A., Sanchez, K. J., Roberts, G., Ceburnis, D., Decesari,
27 S., Rinaldi, M., Hodas, N., Facchini, M. C., Seinfeld, J. H., and Dowd, C. O.: Surface
28 tension prevails over solute effect in organic-influenced cloud droplet activation, *Nature*,
29 546, 637-641, 10.1038/nature22806, 2017.

30 Pajunoja, A., Malila, J., Hao, L. Q., Joutsensaari, J., Lehtinen, K. E. J., and Virtanen, A.:
31 Estimating the viscosity range of SOA particles based on their coalescence time, *Aerosol*
32 *Sci. Tech.*, 48, I-Iv, <https://doi.10.1080/02786826.2013.870325>, 2014.

1 Pandis, S. N., Harley, R. A., Cass, G. R., and Seinfeld, J. H.: Secondary organic aerosol
2 formation and transport, *Atmos. Environ. A-Gen.*, 26, 2269–2282, 1992.

3 Pankow, J. F.: Gas/particle partitioning of neutral and ionizing compounds to single and multi-
4 phase aerosol particles. 1. Unified modeling framework, *Atmos. Environ.*, 37, 3323–3333,
5 [https://doi.org/10.1016/S1352-2310\(03\)00346-7](https://doi.org/10.1016/S1352-2310(03)00346-7), 2003.

6 Pant, A., Parsons, M. T., and Bertram, A. K.: Crystallization of aqueous ammonium sulfate
7 particles internally mixed with soot and kaolinite: Crystallization relative humidities and
8 nucleation rates, *J. Phys. Chem. A*, 110, 8701-8709, <https://doi.10.1021/Jp060985s>, 2006.

9 Parsons, M. T., Mak, J., Lipetz, S. R., and Bertram, A. K.: Deliquescence of malonic, succinic,
10 glutaric, and adipic acid particles, *J. Geophys. Res.-Atmos.*, 109, D06212,
11 <https://doi.org/10.1029/2003jd004075>, 2004.

12 Perraud, V., Bruns, E. A., Ezell, M. J., Johnson, S. N., Yu, Y., Alexander, M. L., Zelenyuk, A.,
13 Imre, D., Chang, W. L., Dabdub, D., Pankow, J. F., and Finlayson-Pitts, B. J.:
14 Nonequilibrium atmospheric secondary organic aerosol formation and growth, *P. Natl.*
15 *Acad. Sci. USA*, 109, 2836-2841, <https://doi.10.1073/pnas.1119909109>, 2012.

16 Petters, M. D., and Kreidenweis, S. M.: A single parameter representation of hygroscopic
17 growth and cloud condensation nucleus activity, *Atmos. Chem. Phys.*, 7, 1961-1971,
18 <https://doi.10.5194/acp-7-1961-2007>, 2007.

19 Petters, M. D., Kreidenweis, S. M., Snider, J. R., Koehler, K. A., Wang, Q., Prenni, A. J., and
20 Demott, P. J.: Cloud droplet activation of polymerized organic aerosol, *Tellus B*, 58, 196-
21 205, DOI 10.1111/j.1600-0889.2006.00181.x, 2006.

22 Pöschl, U., Martin, S. T., Sinha, B., Chen, Q., Gunthe, S. S., Huffman, J. A., Borrmann, S.,
23 Farmer, D. K., Garland, R. M., Helas, G., Jimenez, J. L., King, S. M., Manzi, A., Mikhailov,
24 E., Pauliquevis, T., Petters, M. D., Prenni, A. J., Roldin, P., Rose, D., Schneider, J., Su, H.,
25 Zorn, S. R., Artaxo, P., and Andreae, M. O.: Rainforest aerosols as biogenic nuclei of
26 clouds and precipitation in the Amazon., *Science*, 329, 1513–1516,
27 <https://doi.org/10.1126/science.1191056>, 2010.

28 Pöschl, U., and Shiraiwa, M.: Multiphase Chemistry at the Atmosphere-Biosphere Interface
29 Influencing Climate and Public Health in the Anthropocene, *Chem. Rev.*, 115, 4440-4475,
30 <https://doi.10.1021/cr500487s>, 2015.

31 Price, H. C., Mattsson, J., and Murray, B. J.: Sucrose diffusion in aqueous solution, *Phys. Chem.*
32 *Chem. Phys.*, 18, 19207-19216, <https://doi.10.1039/c6cp03238a>, 2016.

1 Price, H. C., Mattsson, J., Zhang, Y., Bertram, A. K., Davies, J. F., Grayson, J. W., Martin, S.
2 T., O'Sullivan, D., Reid, J. P., Rickards, A. M. J., and Murray, B. J.: Water diffusion in
3 atmospherically relevant alpha-pinene secondary organic material, *Chem. Sci.*, 6, 4876-
4 4883, 10.1039/c5sc00685f, 2015.

5 Pye, H. O. T., Chan, A. W. H., Barkley, M. P., and Seinfeld, J. H.: Global modeling of organic
6 aerosol: the importance of reactive nitrogen (NO_x and NO_3), *Atmos. Chem. Phys.*, 10,
7 11261-11276, 10.5194/acp-10-11261-2010, 2010.

8 Rastak, N., Pajunoja, A., Navarro, J. C. A., Ma, J., Song, M., Partridge, D. G., Kirkevåg, A.,
9 Leong, Y., Hu, W. W., Taylor, N. F., Lambe, A., Cerully, K., Bougiatioti, A., Liu, P., Krejci,
10 R., Petaja, T., Percival, C., Davidovits, P., Worsnop, D. R., Ekman, A. M. L., Nenes, A.,
11 Martin, S., Jimenez, J. L., Collins, D. R., Topping, D. O., Bertram, A. K., Zuend, A.,
12 Virtanen, A., and Riipinen, I.: Microphysical explanation of the RH-dependent water
13 affinity of biogenic organic aerosol and its importance for climate, *Geophys. Res. Lett.*,
14 44, 5167–5177, <https://doi.org/10.1002/2017gl073056>, 2017.

15 Riipinen, I., Pierce, J. R., Yli-Juuti, T., Nieminen, T., Hakkinen, S., Ehn, M., Junninen, H.,
16 Lehtipalo, K., Petaja, T., Slowik, J., Chang, R., Shantz, N. C., Abbatt, J., Leaitch, W. R.,
17 Kerminen, V. M., Worsnop, D. R., Pandis, S. N., Donahue, N. M., and Kulmala, M.:
18 Organic condensation: a vital link connecting aerosol formation to cloud condensation
19 nuclei (CCN) concentrations, *Atmos. Chem. Phys.*, 11, 3865-3878, DOI 10.5194/acp-11-
20 3865-2011, 2011.

21 Reid, J. P., Bertram, A. K., Topping, D. O., Laskin, A., Martin, S. T., Petters, M. D., Pope, F.
22 D., and Rovelli, G.: The viscosity of atmospherically relevant organic particles, *Nat.*
23 *Commun.*, 9, ARTN 956 10.1038/s41467-018-03027-z, 2018.

24 Reid, J. P., Dennis-Smith, B. J., Kwamena, N. O. A., Miles, R. E. H., Hanford, K. L., and
25 Homer, C. J.: The morphology of aerosol particles consisting of hydrophobic and
26 hydrophilic phases: hydrocarbons, alcohols and fatty acids as the hydrophobic component,
27 *Phys. Chem. Chem. Phys.*, 13, 15559–15572, <https://doi.org/10.1039/C1cp21510h>, 2011.

28 Reist, P.: *Aerosol science and technology*, McGraw-Hill Professional, New York, NY, USA, 2
29 Edn., 1992.

30 Renbaum-Wolff, L., Grayson, J. W., Bateman, A. P., Kuwata, M., Sellier, M., Murray, B. J.,
31 Shilling, J. E., Martin, S. T., and Bertram, A. K.: Viscosity of alpha-pinene secondary
32 organic material and implications for particle growth and reactivity, *Proc. Natl. Acad. Sci.*

1 US, 110, 8014-8019, <https://doi.org/10.1073/pnas.1219548110>, 2013.

2 Renbaum-Wolff, L., Song, M., Marcolli, C., Zhang, Y., Liu, P. F., Grayson, J. W., Geiger, F. M.,
3 Martin, S. T., and Bertram, A. K.: Observations and implications of liquid-liquid phase
4 separation at high relative humidities in secondary organic material produced by α -pinene
5 ozonolysis without inorganic salts, *Atmos. Chem. Phys.*, 16, 7969–7979,
6 <https://doi.org/10.5194/acp16-7969-2016>, 2016.

7 Roach, P. J., Laskin, J., and Laskin, A.: Molecular characterization of organic aerosols using
8 nanospray-desorption/electrospray ionization-mass spectrometry, *Anal. Chem.*, 82, 7979-
9 7986, 10.1021/ac101449p, 2010.

10 Robinson, E. S., Saleh, R., and Donahue, N. M.: Organic aerosol mixing observed by single-
11 particle mass spectrometry, *J. Phys. Chem. A*, 117, 13935-13945,
12 <https://doi.10.1021/Jp405789t>, 2013.

13 Rothfuss, N. E., and Petters, M. D.: Influence of functional groups on the viscosity of organic
14 aerosol, *Environ. Sci. Technol.*, 51, 271-279, 10.1021/acs.est.6b04478, 2017.

15 Saukko, E., Lambe, A. T., Massoli, P., Koop, T., Wright, J. P., Croasdale, D. R., Pedernera, D.
16 A., Onasch, T. B., Laaksonen, A., Davidovits, P., Worsnop, D. R., and Virtanen, A.:
17 Humidity-dependent phase state of SOA particles from biogenic and anthropogenic
18 precursors, *Atmos. Chem. Phys.*, 12, 7517-7529, <https://doi.10.5194/acp-12-7517-2012>,
19 2012.

20 Schauer, J. J., Fraser, M. P., Cass, G. R., and Simoneit, B. R. T.: Source reconciliation of
21 atmospheric gas-phase and particle-phase pollutants during a severe photochemical smog
22 episode, *Environ. Sci. Technol.*, 36, 3806-3814, <https://doi.10.1021/Es011458j>, 2002a.

23 Schauer, J. J., Kleeman, M. J., Cass, G. R., and Simoneit, B. R. T.: Measurement of emissions
24 from air pollution sources. 5. C-1-C-32 organic compounds from gasoline-powered motor
25 vehicles, *Environ. Sci. Technol.*, 36, 1169-1180, <https://doi.10.1021/Es0108077>, 2002b.

26 Schill, G. P., De Haan, D. O., and Tolbert, M. A.: Heterogeneous ice nucleation on simulated
27 secondary organic aerosol, *Environ. Sci. Technol.*, 48, 1675-1682, 2014.

28 Seinfeld, J. H., and Pandis, S. N.: *Atmospheric chemistry and physics*, A Wiley-interscience
29 publication, 2006.

30 Shiraiwa, M., Ammann, M., Koop, T., and Poschl, U.: Gas uptake and chemical aging of
31 semisolid organic aerosol particles, *Proc. Natl. Acad. Sci. US*, 108, 11003-11008,
32 <https://doi.10.1073/pnas.1103045108>, 2011.

1 Shiraiwa, M., and Seinfeld, J. H.: Equilibration timescale of atmospheric secondary organic
2 aerosol partitioning, *Geophys. Res. Lett.*, 39, L24801, <https://doi.10.1029/2012gl054008>,
3 2012.

4 Shiraiwa, M., Yee, L. D., Schilling, K. A., Loza, C. L., Craven, J. S., Zuend, A., Ziemann, P. J.,
5 and Seinfeld, J. H.: Size distribution dynamics reveal particle-phase chemistry in organic
6 aerosol formation, *Proc. Natl. Acad. Sci. USA*, 110, 11746-11750,
7 <https://doi.10.1073/pnas.1307501110>, 2013.

8 Shiraiwa, M., Zuend, A., Bertram, A. K., and Seinfeld, J. H.: Gas particle partitioning of
9 atmospheric aerosols: interplay of physical state, non-ideal mixing and morphology, *Phys.*
10 *Chem. Chem. Phys.*, 15, 11441–11453, <https://doi.org/10.1039/C3cp51595h>, 2013.

11 Shiraiwa, M., Li, Y., Tsimpidi, A. P., Karydis, V. A., Berkemeier, T., Pandis, S. N., Lelieveld,
12 J., Koop, T., and Poschl, U.: Global distribution of particle phase state in atmospheric
13 secondary organic aerosols, *Nat. Commun.*, 8, 15002, <https://doi.10.1038/ncomms15002>,
14 2017.

15 Shrivastava, M., Cappa, C. D., Fan, J. W., Goldstein, A. H., Guenther, A. B., Jimenez, J. L.,
16 Kuang, C., Laskin, A., Martin, S. T., Ng, N. L., Petaja, T., Pierce, J. R., Rasch, P. J., Roldin,
17 P., Seinfeld, J. H., Shilling, J., Smith, J. N., Thornton, J. A., Volkamer, R., Wang, J.,
18 Worsnop, D. R., Zaveri, R. A., Zelenyuk, A., and Zhang, Q.: Recent advances in
19 understanding secondary organic aerosol: Implications for global climate forcing, *Rev.*
20 *Geophys.*, 55, 509-559, [10.1002/2016rg000540](https://doi.10.1002/2016rg000540), 2017.

21 Shrivastava, M., Lou, S., Zelenyuk, A., Easter, R. C., Corley, R. A., Thrall, B. D., Rasch, P. J.,
22 Fast, J. D., Simonich, S. L. M., Shen, H. Z., and Tao, S.: Global long-range transport and
23 lung cancer risk from polycyclic aromatic hydrocarbons shielded by coatings of organic
24 aerosol, *Proc. Natl. Acad. Sci. US*, 114, 1246-1251, [10.1073/pnas.1618475114](https://doi.10.1073/pnas.1618475114), 2017.

25 Solomon, S.: *Climate change 2007-the physical science basis: Working group I contribution to*
26 *the fourth assessment report of the IPCC*, Cambridge University Press, 2007.

27 Song, M., Marcolli, C., Krieger, U. K., Zuend, A., and Peter, T.: LLPS and morphology of
28 internally mixed dicarboxylic acids/ammonium sulfate/water particles, *Atmos. Chem.*
29 *Phys.*, 12, 2691-2712, <https://doi.10.5194/acp-12-2691-2012>, 2012a.

30 Song, M., Marcolli, C., Krieger, U. K., Zuend, A., and Peter, T.: Liquid-liquid phase separation
31 in aerosol particles: Dependence on O: C, organic functionalities, and compositional
32 complexity, *Geophys. Res. Lett.*, 39, L19801, <https://doi.org/10.1029/2012gl052807>,

1 2012b.

2 Song, M. J., Marcolli, C., Krieger, U. K., Lienhard, D. M., and Peter, T.: Morphologies of
3 mixed organic/inorganic/aqueous aerosol droplets, *Faraday Discuss.*, 165, 289-316,
4 <https://doi.10.1039/C3fd00049d>, 2013.

5 Song, M., Liu, P. F., Hanna, S. J., Li, Y. J., Martin, S. T., and Bertram, A. K.: RH-dependent
6 viscosities of isoprene-derived secondary organic material and atmospheric implications
7 for isoprene-dominant forests, *Atmos. Chem. Phys.*, 15, 5145-5159, 2015.

8 Song, M., Liu, P. F. F., Hanna, S. J., Zaveri, R. A., Potter, K., You, Y., Martin, S. T., and Bertram,
9 A. K.: RH-dependent viscosity of secondary organic material from toluene photo-
10 oxidation and possible implications for organic particulate matter over megacities, *Atmos.*
11 *Chem. Phys.*, 16, 8817-8830, [10.5194/acp-16-8817-2016](https://doi.org/10.5194/acp-16-8817-2016), 2016a.

12 Song, Y. C., Haddrell, A. E., Bzdek, B. R., Reid, J. P., Barman, T., Topping, D. O., Percival, C.,
13 and Cai, C.: Measurements and predictions of binary component aerosol particle viscosity,
14 *J. Phys. Chem. A*, 120, 8123-8137, [10.1021/acs.jpca.6b07835](https://doi.org/10.1021/acs.jpca.6b07835), 2016b.

15 Song, M., Liu, P., Martin, S. T., Bertram, A. K.: Liquid–liquid phase separation in particles
16 containing secondary organic material free of inorganic salts, *Atmos. Chem. Phys.*, 17,
17 11261-11271, <https://doi.org/10.5194/acp-17-11261-2017>, 2017.

18 Song, M., Ham, S., Andrews, R. J., You, Y., Bertram, A. K.: Liquid–liquid phase separation in
19 organic particles containing one and two organic species: importance of the average O: C,
20 *Atmos. Chem. Phys.*, 18, 12075-12084, <https://doi.org/10.5194/acp-18-12075-2018>, 2018.

21 Steimer, S. S., Lampimaki, M., Coz, E., Grzinic, G., and Ammann, M.: The influence of
22 physical state on shikimic acid ozonolysis: a case for in situ microspectroscopy, *Atmos.*
23 *Chem. Phys.*, 14, 10761-10772, 2014.

24 Ullmann, D. A., Hinks, M. L., Maclean, A. M., Butenhoff, C. L., Grayson, J. W., Barsanti, K.,
25 Jimenez, J. L., Nizkorodov, S. A., Kamal, S., and Bertram, A. K.: Viscosities, diffusion
26 coefficients, and mixing times of intrinsic fluorescent organic molecules in brown
27 limonene secondary organic aerosol and tests of the Stokes–Einstein equation, *Atmos.*
28 *Chem. Phys.*, 19, 1491-1503, <https://doi.org/10.5194/acp-19-1491-2019>, 2019.

29 Veghte, D. P., Altaf, M. B., and Freedman, M. A.: Size dependence of the structure of organic
30 aerosol, *J. Am. Chem. Soc.*, 135, 16046–16049, [10.1021/ja408903g](https://doi.org/10.1021/ja408903g), 2013.

31 Velasco, E., Lamb, B., Westberg, H., Allwine, E., Sosa, G., Arriaga-Colina, J. L., Jobson, B. T.,
32 Alexander, M. L., Prazeller, P., Knighton, W. B., Rogers, T. M., Grutter, M., Herndon, S.

1 C., Kolb, C. E., Zavala, M., de Foy, B., Volkamer, R., Molina, L. T., and Molina, M. J.:
2 Distribution, magnitudes, reactivities, ratios and diurnal patterns of volatile organic
3 compounds in the Valley of Mexico during the MCMA 2002 & 2003 field campaigns,
4 *Atmos. Chem. Phys.*, 7, 329-353, 2007.

5 Velasco, E., Pressley, S., Grivicke, R., Allwine, E., Coons, T., Foster, W., Jobson, B. T.,
6 Westberg, H., Ramos, R., Hernandez, F., Molina, L. T., and Lamb, B.: Eddy covariance
7 flux measurements of pollutant gases in urban Mexico City, *Atmos. Chem. Phys.*, 9, 7325-
8 7342, 2009.

9 Virtanen, A., Joutsensaari, J., Koop, T., Kannosto, J., Yli-Pirila, P., Leskinen, J., Makela, J. M.,
10 Holopainen, J. K., Poschl, U., Kulmala, M., Worsnop, D. R., and Laaksonen, A.: An
11 amorphous solid state of biogenic secondary organic aerosol particles, *Nature*, 467, 824-
12 827, 10.1038/nature09455, 2010.

13 Vutukuru, S., Griffin, R. J., and Dabdub, D.: Simulation and analysis of secondary organic
14 aerosol dynamics in the South Coast Air Basin of California, *J. Geophys. Res.-Atmos.*,
15 111, 2006.

16 Wang, B. B., Lambe, A. T., Massoli, P., Onasch, T. B., Davidovits, P., Worsnop, D. R., and
17 Knopf, D. A.: The deposition ice nucleation and immersion freezing potential of
18 amorphous secondary organic aerosol: Pathways for ice and mixed-phase cloud formation,
19 *J. Geophys. Res.-Atmos.*, 117, D16209, <https://doi.10.1029/2012jd018063>, 2012.

20 Wang, B. B., O'Brien, R. E., Kelly, S. T., Shilling, J. E., Moffet, R. C., Gilles, M. K., and Laskin,
21 A.: Reactivity of liquid and semisolid secondary organic carbon with chloride and nitrate
22 in atmospheric aerosols, *J. of Phys. Chem. A*, 119, 4498-4508, 2015.

23 Wang, L. N., Cai, C., and Zhang, Y. H.: Kinetically determined hygroscopicity and
24 efflorescence of sucrose-ammonium sulfate aerosol droplets under lower RH, *J. Phys.*
25 *Chem. B*, 121, 8551-8557, 10.1021/acs.jpcc.7b05551, 2017.

26 **Wilson, J., Imre, D., Beranek, J., Shrivastava, M., and Zelenyuk, A.: Evaporation Kinetics of**
27 **Laboratory-Generated Secondary Organic Aerosols at Elevated Relative Humidity,**
28 ***Environ. Sci. Technol.*, 49, 243-249, 10.1021/es505331d, 2015.**

29 Wilson, T. W., Murray, B. J., Wagner, R., Mohler, O., Saathoff, H., Schnaiter, M., Skrotzki, J.,
30 Price, H. C., Malkin, T. L., Dobbie, S., and Al-Jumur, S. M. R. K.: Glassy aerosols with a
31 range of compositions nucleate ice heterogeneously at cirrus temperatures, *Atmos. Chem.*
32 *Phys.*, 12, 8611-8632, 2012.

- 1 Ye, Q., Robinson, E. S., Ding, X., Ye, P. L., Sullivan, R. C., and Donahue, N. M.: Mixing of
2 secondary organic aerosols versus relative humidity, *Proc. Natl. Acad. Sci. US*, 113,
3 12649-12654, 10.1073/pnas.1604536113, 2016.
- 4 Ye, Q., Upshur, M. A., Robinson, E. S., Geiger, F. M., Sullivan, R. C., Thomson, R. J., and
5 Donahue, N. M.: Following particle-particle mixing in atmospheric secondary organic
6 aerosols by using isotopically labeled terpenes, *Chem.-Us*, 4, 318-333,
7 10.1016/j.chempr.2017.12.008, 2018.
- 8 Yli-Juuti, T., Pajunoja, A., Tikkanen, O. P., Buchholz, A., Faiola, C., Vaisanen, O., Hao, L. Q.,
9 Kari, E., Perakyla, O., Garmash, O., Shiraiwa, M., Ehn, M., Lehtinen, K., and Virtanen,
10 A.: Factors controlling the evaporation of secondary organic aerosol from alpha-pinene
11 ozonolysis, *Geophys. Res. Lett.*, 44, 2562-2570, 10.1002/2016gl072364, 2017.
- 12 You, Y., Smith, M. L., Song, M. J., Martin, S. T., and Bertram, A. K.: Liquid-liquid phase
13 separation in atmospherically relevant particles consisting of organic species and inorganic
14 salts, *Int. Rev. Phys. Chem.*, 33, 43–77, <https://doi.org/10.1080/0144235X.2014.890786>,
15 2014.
- 16 Zaveri, R. A., Easter, R. C., Shilling, J. E., and Seinfeld, J. H.: Modeling kinetic partitioning of
17 secondary organic aerosol and size distribution dynamics: representing effects of volatility,
18 phase state, and particle-phase reaction, *Atmos. Chem. Phys.*, 14, 5153-5181,
19 <https://doi.10.5194/acp-14-5153-2014>, 2014.
- 20 Zaveri, R. A., Shilling, J. E., Zelenyuk, A., Liu, J. M., Bell, D. M., D'Ambro, E. L., Gaston, C.,
21 Thornton, J. A., Laskin, A., Lin, P., Wilson, J., Easter, R. C., Wang, J., Bertram, A. K.,
22 Martin, S. T., Seinfeld, J. H., and Worsnop, D. R.: Growth kinetics and size distribution
23 dynamics of viscous secondary organic aerosol, *Environ. Sci. Technol.*, 52, 1191-1199,
24 10.1021/acs.est.7b04623, 2018.
- 25 Zelenyuk, A., Imre, D., Beranek, J., Abramson, E., Wilson, J., and Shrivastava, M.: Synergy
26 between secondary organic aerosols and long-range transport of polycyclic aromatic
27 hydrocarbons, *Environ. Sci. Technol.*, 46, 12459-12466, <https://doi.10.1021/Es302743z>,
28 2012.
- 29 Zhang, Q., Jimenez, J. L., Canagaratna, M. R., Allan, J. D., Coe, H., Ulbrich, I., Alfarra, M. R.,
30 Takami, A., Middlebrook, A. M., Sun, Y. L., Dzepina, K., Dunlea, E., Docherty, K.,
31 DeCarlo, P. F., Salcedo, D., Onasch, T., Jayne, J. T., Miyoshi, T., Shimonono, A., Hatakeyama,
32 S., Takegawa, N., Kondo, Y., Schneider, J., Drewnick, F., Borrmann, S., Weimer, S.,

1 Demerjian, K., Williams, P., Bower, K., Bahreini, R., Cottrell, L., Griffin, R. J., Rautiainen,
2 J., Sun, J. Y., Zhang, Y. M., and Worsnop, D. R.: Ubiquity and dominance of oxygenated
3 species in organic aerosols in anthropogenically-influenced Northern Hemisphere
4 midlatitudes, *Geophys. Res. Lett.*, 34, L13801, <https://doi.10.1029/2007gl029979>, 2007.

5 Zhang, Y., Chen, Y. Z., Lambe, A. T., Olson, N. E., Lei, Z. Y., Craig, R. L., Zhang, Z. F., Gold,
6 A., Onasch, T. B., Jayne, J. T., Worsnop, D. R., Gaston, C. J., Thornton, J. A., Vizuete, W.,
7 Ault, A. P., and Surratt, J. D.: Effect of the aerosol-phase state on secondary organic aerosol
8 formation from the reactive uptake of isoprene-derived epoxydiols (IEPDX), *Environ. Sci.*
9 *Tech. Lett.*, 5, 167-174, [10.1021/acs.estlett.8b00044](https://doi.10.1021/acs.estlett.8b00044), 2018.

10 Zhang, Y., Sanchez, M. S., Douet, C., Wang, Y., Bateman, A. P., Gong, Z., Kuwata, M.,
11 Renbaum-Wolff, L., Sato, B. B., Liu, P. F., Bertram, A. K., Geiger, F. M., and Martin, S.
12 T.: Changing shapes and implied viscosities of suspended submicron particles, *Atmos.*
13 *Chem. Phys.*, 15, 7819-7829, [10.5194/acp-15-7819-2015](https://doi.10.5194/acp-15-7819-2015), 2015.

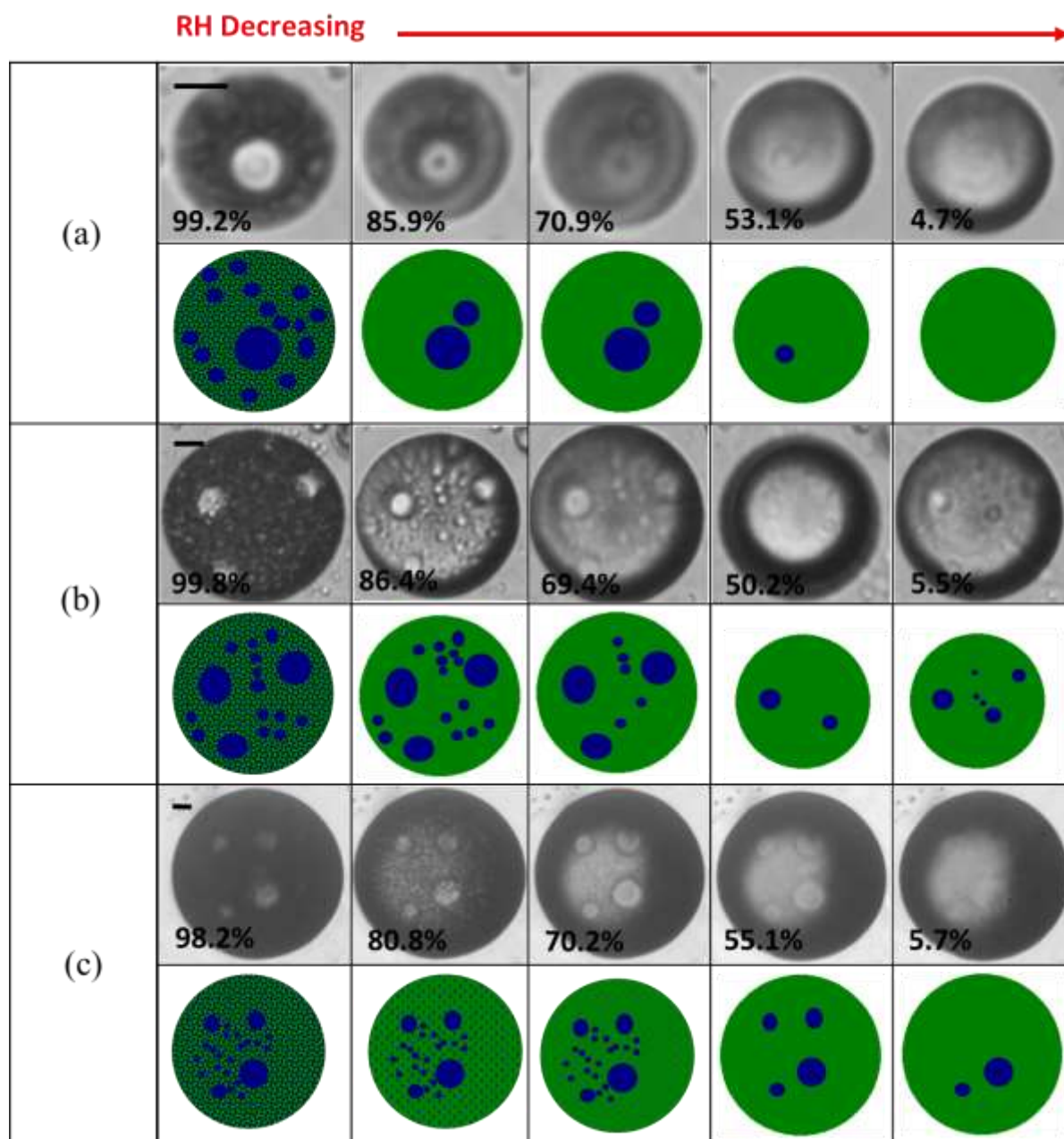
14 Zhou, S. M., Shiraiwa, M., McWhinney, R. D., Poschl, U., and Abbatt, J. P. D.: Kinetic
15 limitations in gas-particle reactions arising from slow diffusion in secondary organic
16 aerosol, *Faraday Discuss.*, 165, 391-406, <https://doi.10.1039/C3fd00030c>, 2013.

17 Zobrist, B., Marcolli, C., Pedernera, D. A., and Koop, T.: Do atmospheric aerosols form
18 glasses?, *Atmos. Chem. Phys.*, 8, 5221-5244, 2008.

19 Zuend, A. and Seinfeld, J. H.: Modeling the gas-particle partitioning of secondary organic
20 aerosol: the importance of liquid-liquid phase separation, *Atmos. Chem. Phys.*, 12, 3857–
21 3882, <https://doi.org/10.5194/acp-12-3857-2012>, 2012.

22 Zuend, A., Marcolli, C., Peter, T., and Seinfeld, J. H.: Computation of liquid-liquid equilibria
23 and phase stabilities: implications for RH-dependent gas/particle partitioning of organic
24 inorganic aerosols, *Atmos. Chem. Phys.*, 10, 7795–7820, [https://doi.org/10.5194/acp-10-](https://doi.org/10.5194/acp-10-7795-2010)
25 [7795-2010](https://doi.org/10.5194/acp-10-7795-2010), 2010.

26



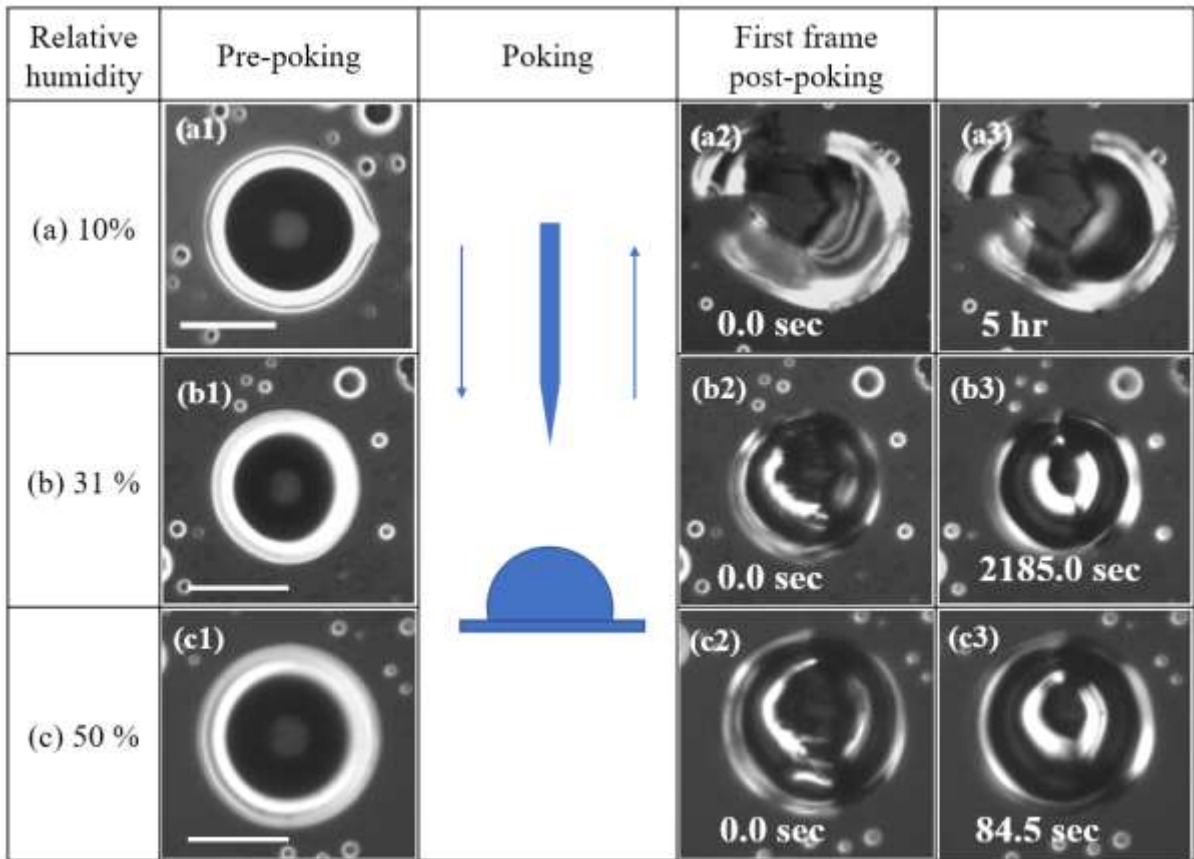
1

2

3 Figure 1. Optical images and illustrations of three diesel fuel SOA particles taken while the RH
 4 was decreased. Illustrations are provided to help interpret the optical images with green color
 5 representing the organic-rich phase, and blue color representing the water-rich phase. The
 6 numbers under the optical images indicate the RH. The length of the scale bar is 10 μm .

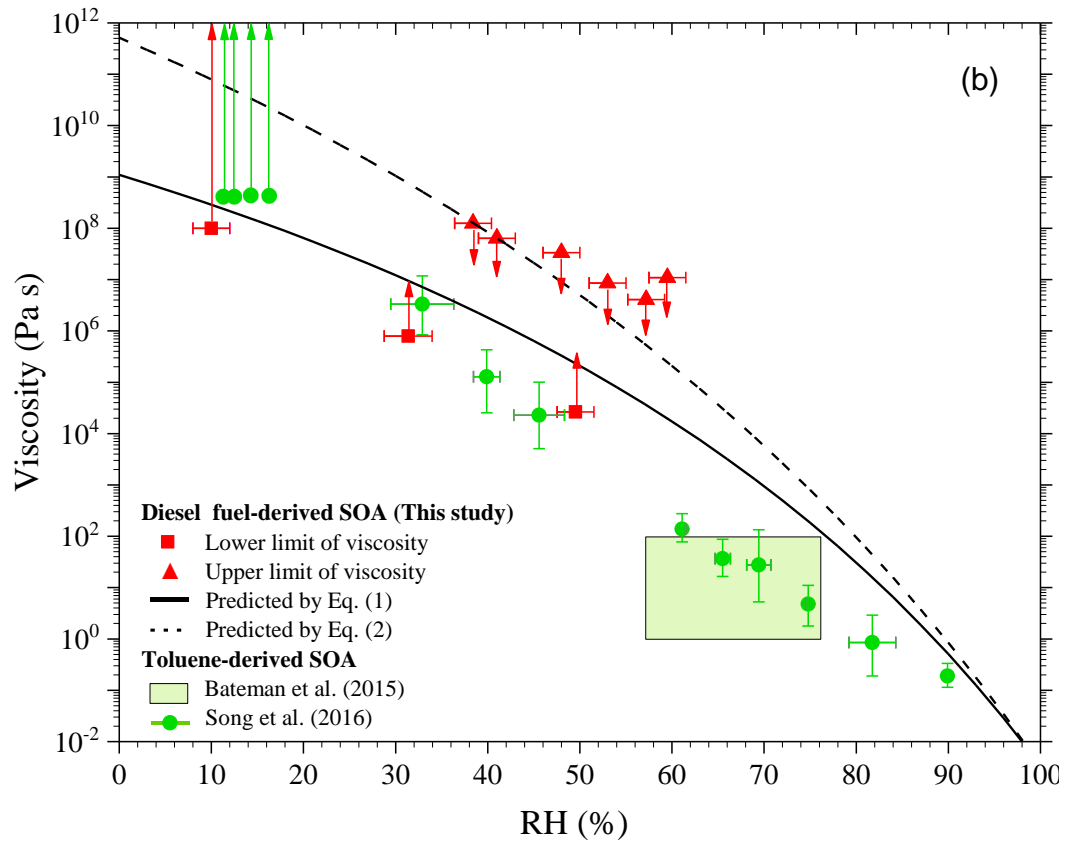
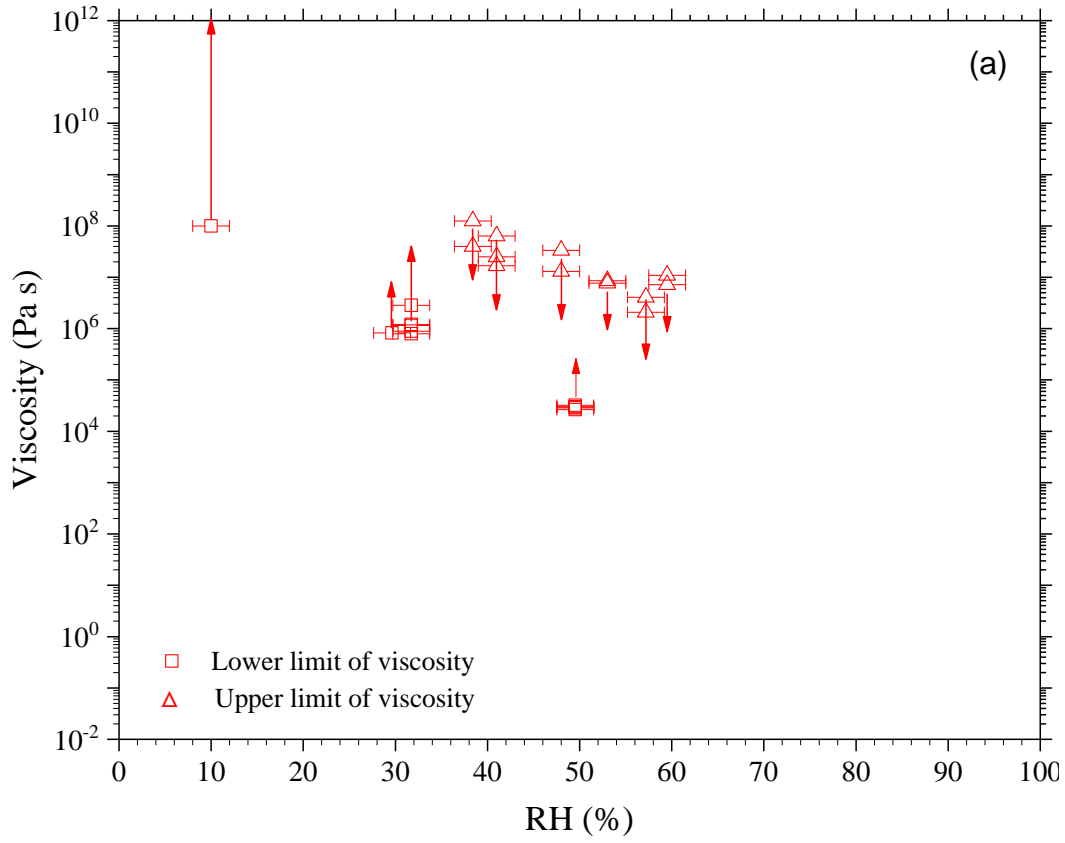
7

8



1
2
3
4
5
6
7

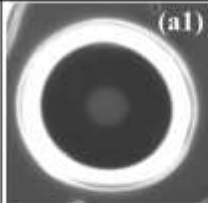
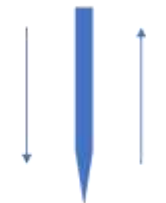
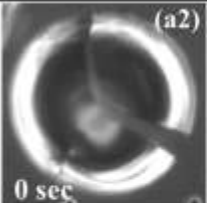
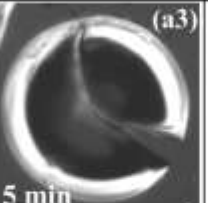
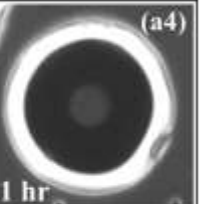
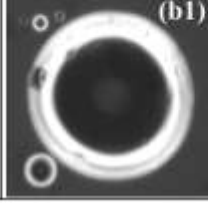

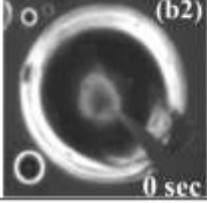
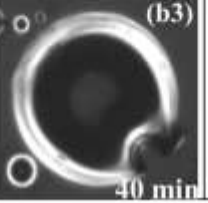
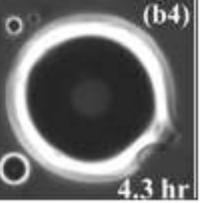
Figure 2. Optical images of SOA particles during a poke-and-flow experiment: (a) 10 % RH, (b) 31 % RH, and (c) 50 % RH. The size of the scale bar is 20 μm .



1

2 Figure 3. (a) Viscosities of diesel fuel SOA. Each data point corresponds to a viscosity
3 determined from poking a single and different particle. Each particle was prepared with the
4 same reaction conditions. Upward arrows indicate lower limit to the viscosities and downward
5 arrows indicate upper limit to the viscosities of diesel fuel SOA. The x error bars represent
6 uncertainty in the RH measurements. (b) Viscosities of diesel fuel-derived SOA but with the
7 viscosities from individual poke-and-flow experiments grouped by RH. The lower limit to the
8 viscosities and the upper limit to the viscosities represent the lowest and the highest viscosities
9 in the group, respectively. At least two data points were included in each group. The x error
10 bars represent the lowest and highest RH ranges in the group and the uncertainty in the RH
11 measurements. Also included are viscosities of toluene SOA from Bateman et al. (2015) (green
12 box) and Song et al. (2016) (green circle) and predicted viscosities of the diesel fuel SOA using
13 Eq. (1) (black solid line) and Eq. (2) (black dashed line).

14

Relative humidity	Pre-poking	Poking	First frame post-poking	During recovery	$\tau_{exp, recovery}$
(a) 53%					
(b) 38%					

1

2

3 Figure 4. Optical images of diesel fuel SOA particles during poke-and-flow experiments. In
 4 these experiments the SOA particles were poked at 0 % RH and then exposed to RH values of
 5 53% (a) and 38% (b). The last column shows the particles after they have returned to a spherical
 6 cap shape.

7

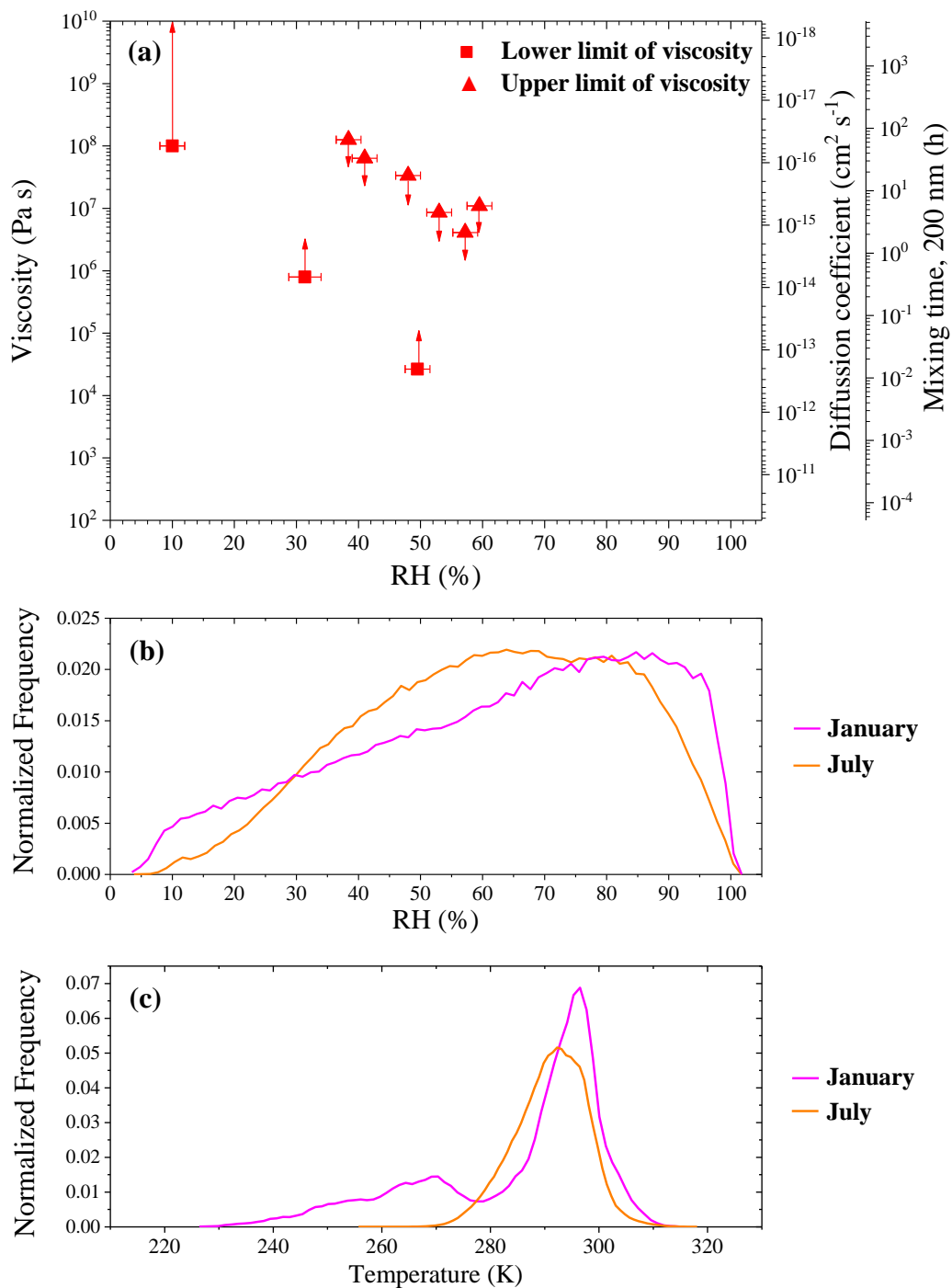
8

9

10

11

12



1
2

3 Figure 5. Panel (a): Viscosities, diffusion coefficients, and mixing times of organic molecules
4 within 200 nm diesel fuel SOA. Panel b and c represent the RH frequency distribution and the
5 temperature frequency distribution in the planetary boundary layer when the average
6 concentrations of organic aerosol are higher than 0.5 $\mu\text{g m}^{-3}$ at the surface based on GEOS-
7 Chem (Ullmann et al., 2018). The frequency distributions were calculated using monthly mean

1 meteorological data from GEOS-Chem version v10-01 and data was only included when the
2 monthly mean concentrations of organic aerosol at the surface were greater than $0.5 \mu\text{g m}^{-3}$
3 (Maclean et al., 2017).